Biomechanics and Modeling in Mechanobiology
https://doi.org/10.1007/s10237-018-01112-2

ORIGINAL PAPER

The effect of fibrillar degradation on the mechanics of articular cartilage: a computational model

Tanvir R. Faisal[1,2,5] · **Malek Adouni**[4] · **Yasin Y. Dhaher**[1,2,3]

Received: 26 June 2018 / Accepted: 20 December 2018

Abstract

The pathogenesis and pathophysiological underpinnings of cartilage degradation are not well understood. Either mechanically or enzymatically mediated degeneration at the fibril level can lead to acute focal injuries that will, overtime, cause significant cartilage degradation. Understanding the relationship between external loading and the basic molecular structure of cartilage requires establishing a connection between the fibril-level defects and its aggregate effect on cartilage. In this work, we provide a multiscale constitutive model of cartilage to elucidate the effect of two plausible fibril degradation mechanisms on the aggregate tissue: tropocollagen crosslink failure (β) and a generalized surface degradation (δ). Using our model, the mechanics of aggregate tissue shows differed yield stress and post-yield behavior after crosslink failure and surface degradation compared to intact cartilage, and the tissue-level aggregate behaviors are different from the fibrillar behaviors observed in the molecular dynamics simulations. We also compared the effect of fibrillar defects in terms of crosslink failure and surface degradation in different layers of cartilage within the macroscale tissue construct during a simulated nanoindentation test. Although the mechanical properties of cartilage tissue were largely contingent upon the mechanical properties of the fibril, the macroscale mechanics of cartilage tissue showed ~ 10% variation in yield strain (tissue yield strain: ~ 27 to ~ 37%) compared to fibrillar yield strain (fibrillar yield strain: ~ 16 to ~ 26%) for crosslink failure and ~ 7% difference for the surface degradation (yield strain variations at the tissue: ~ 30 to ~ 37% and fibril: ~ 24 to ~ 26%) at the superficial layer. The yield strain was further delayed in middle layers at least up to 30% irrespective of the failure mechanisms. The cartilage tissue appeared to withstand more strain than the fibrils. The degeneration mechanisms of fibril differentially influenced the aggregate mechanics of cartilage, and the deviation may be attributed to fiber–matrix interplay, depth-dependent fiber orientation and fibrillar defects with different degradation mechanisms. The understanding of the aggregate stress–strain behavior of cartilage tissue, cartilage degradation and its underlying biomechanical factors is important for developing engineering approaches and therapeutic interventions for cartilage pathologies.

Keywords Cartilage degradation · Crosslink failure · Surface degradation · Multiscale modeling

1 Introduction

Recent studies show that knee joint and cartilage injuries and subsequent degenerative disease are leading sources of long-term disability in the USA (Centers for Disease Control and Prevention). Individuals who sustain knee injury are approximately 4.2 times more likely to develop osteoarthritis (OA) compared to those without a history of injury (Muthuri et al. 2011), and post-traumatic OA (PTOA) causes 10% of knee OA (Brown et al. 2006). After an injury or trauma, pro-inflammatory molecules activate degradative enzymes in the cartilage, reducing its mechanical properties and wear resistance (Backus et al. 2011; Haut et al. 1995; Lotz 2001; Newberry et al. 1998).

✉ Tanvir R. Faisal
tanvir.faisal@louisiana.edu

1 Department of Physical Medicine and Rehabilitation, Northwestern University, Chicago, IL, USA

2 Legs + Walking Lab, Shirley Ryan AbilityLab, Chicago, IL 60611, USA

3 Department of Biomedical Engineering, Northwestern University, Evanston, IL, USA

4 Department of Mechanical Engineering, Australian College of Kuwait, East Meshrif, Kuwait

5 Department of Mechanical Engineering, University of Louisiana at Lafayette, Lafayette, LA 70508, USA

Published online: 02 January 2019

Trauma to the cartilage may also induce mechanical cracks and microstructural damage at the injury sites, originating on the cartilage surface and extending to superficial, middle and deep zones (Atkinson et al. 1998; Haut et al. 1995; Repo and Finlay 1977; Thompson et al. 1991, 1993).

The process of OA progression is multifactorial and has been described microscopically in terms of the depletion of proteoglycan and the breakdown of collagen fibrils networks, which leads to failure of the articular cartilage (Julkunen et al. 2013). Currently there are no effective treatments to slow down or cure articular cartilage degradation in OA until the damaged joint is reconstructed surgically. Knowing the structures and functional mechanisms associated with the relative contribution of the two key constituents (proteoglycan and collagen fibrils network) could significantly influence intervention strategies and improve healthcare solutions.

Research indicates that transient increase in the nano-stiffness of the collagen fibril network at the articular surface during OA initiation is expressed prior to loss of microarchitectural integrity of articular cartilage (Stolz et al. 2004). Using a guinea pigs OA model, Huebner et al. (2010) reported increased collagen fibril cleavage prior to proteoglycan loss and articular surface fibrillation in a cartilage with OA. Thus, it is likely that the change in collagen fibrils network stiffness in the initial stage of OA could be a result of alterations in the individual collagen fibril mechanics rather than proteoglycan loss (extracellular matrix (ECM) degradation), as has been initially proposed (Stolz et al. 2009). Investigations of the mechanical properties of individual collagen fibrils will allow for a better understanding of OA onset. Molecular dynamics (MD) simulations allow us to determine the contribution of the breakdown of collagen fibrils network and its complex microarchitecture that influences the cartilage mechanical response.

It has been proposed that cartilage stiffness is hierarchically contingent upon the collagen fibril, which demonstrates degeneration when loaded beyond yield point (Buehler 2006, 2008). The structural properties are influenced by the surface quality of fibrils (Panwar et al. 2013, 2015) and by the amount of tropocollagen (TC) crosslink (Kaukinen et al. 2005; Tang et al. 2010; Verzijl et al. 2002). However, how changes in these fibril structural properties are manifested in the mechanics at tissue-level, pre- and post-yield remains largely unexplored. Thus, the objective of this study was to characterize the connection between tissue- and fibril-level mechanics in articular cartilage. We hypothesized that the integrity of fiber plays a significant role in the expression of tissue-level yield in the absence of a degraded matrix. We further hypothesize that the stabilizing effect of a nondegraded ECM at the tissue level depends on the degradation type experience by the fibrils.

2 Materials and methods

The current construct has been developed based on the hierarchical morphology observed in collagenous tissue (Adouni and Dhaher 2016; Tang et al. 2009). The continuum-level response of cartilage tissue was modeled hierarchically allowing for a bottom-up formulation, whereby fibrils are embedded in bundle with neo-Hookean matrix to form fibers, and aggregate fibers are embedded in neo-Hookean matrix to form the cartilage tissue (Fig. 7 in "Appendix A"). The cartilage is essentially a fiber-reinforced composite, while the fiber is a fibril-reinforced composite at smaller length scale. In the current modeling approach, we assumed that the properties of matrix within fibers or tissue do not change and the degradation selectively happened to the fibrils not in the matrix. To develop our computation model, we incorporated results from molecular dynamic (MD) simulations of fibril degradation (Malaspina et al. 2017) into a hyperelastoplastic fiber-reinforced model of the cartilage (Adouni and Dhaher 2016). Two plausible (microstructural) fibril degradation mechanisms were examined: tropocollagen crosslink failure (β) such that $\beta = 100 - \beta_o$, where β_o denotes the percentage of intact crosslinks, and a generalized surface degradation (δ). An axisymmetric finite element (FE) model under indentation resembling cartilage samples (plug) used in the reported experimental testing paradigms (Kerin et al. 1998; Spahn et al. 2007) was simulated. The number of experiments targeting indentation-based failure mechanisms for cartilage specimens is limited. With the lonely two studies cited in the current manuscript, we opted to simulate both experiments since the indenter-to-plug size (radius) ratios were different. The rationality behind our attempt to simulate both experiments was to increase the fidelity of our model. Indentation induces nonuniform strain, where both the magnitude and spatial distribution of strain depend on a number of variables, including indentation depth and geometry, size of the cartilage plug (Bae et al. 2007), shown experimentally (Bae et al. 2006; Oyen et al. 2012) and computationally (Hayes et al. 1972). Using the different constructs allowed for interrogation of our model to predict result. In the model, fiber directions expressed depth-dependent spatial orientation, starting at the deep zone where collagen fibers are perpendicular to the subchondral bone and the curve gradually (mid zone) to merge parallel (superficial zone) to the surface (Bi et al. 2005; Julkunen et al. 2008). Due to the lack of experimental data linking changes in cartilage mechanics and the degradation-induced change in fibril mechanical properties, simulation results of the degraded cartilage model were compared with changes in the aggregate cartilage modulus post-collagenase treatment (Laasanen et al. 2003).

2.1 Softening hyperelasticity approach

The mechanical properties and stress–strain relationship of the native collagen fibril can be explored through either experimental methods (Bozec and Horton 2005; Miyazaki and Hayashi 1999) or through molecular dynamics (MD) simulations (Buehler 2006, 2008; Depalle et al. 2016). The connection between structural changes due to degradation and the mechanical properties of the native collagen fibrils are often elusive. In this context, MD simulations are advantageous because the formulation allows for linking molecular details to macroscopic behavior under the normal and degraded states. Malaspina et al. have recently investigated the elastoplastic behavior of the fibril considering coarse-graining approach to get insights into the basic mechanics at the fibril level in response to degradation (Malaspina et al. 2017). The two degradation mechanisms investigated were crosslink failure and surface degradation. The failure of crosslink was simulated by the random removal of all possible enzymatic crosslinks from the native fibril containing 100% crosslinks (β_o). The surface degradation was imitated by cleaving tropocollagen beads at random from the intact fibril surface, emulating the aggregate effect of MMP-mediated degradation. During the surface degradation, the number of crosslinks remained above 94% due to the large number of cleavable sites. Crosslink failure (β) was simulated by the random removal of crosslinks from 100% (native fibril) to 0% in intervals of 20% while keeping all tropocollagen beads intact. The surface was degraded up to 3.3%, where the percentage of surface degradation (δ) was represented as the ratio between the removed bead and the total beads in the fibril. Malaspina and colleagues MD coarse-grained model computed the fibril yield strengths $\left(\sigma^{fl}_{y(\beta)} \text{ and } \sigma^{fl}_{y(\delta)}\right)$ at different crosslink failure (β) and generalized surface degradation (δ) levels (Malaspina et al. 2017).

2.2 Hierarchical constitutive model

The collagen fiber was modeled as the fiber (fibril)-reinforced composites, including the descriptions of fibril mechanics and incompressible neo-Hookean matrix, consistent with the hierarchical presentation described by Adouni and Dhaher (2016). In this multiscale construct, the multiplicative decomposition of the deformation gradient, $\mathbf{F}$, was utilized to describe the interplay between the elastic and plastic responses (Asaro and Rice 1977; Lee 1969), where $\mathbf{F} = \mathbf{F}_e\mathbf{F}_p$; e and p denote elastic and plastic components; and λ_{fe} and λ_{fp} denote elastic and plastic principal fibril stretch, respectively. The strain invariants in general are $I_1 = \lambda_1^2 + 2\lambda_1^{-1}$ and $I_4 = \mathbf{C} : \mathbf{n}_o \otimes \mathbf{n}_o = \lambda_f^2 = \lambda_1^2 = \lambda^2$. In the current hierarchical construct, it was assumed that λ_f is always directed toward the principle strain λ_1 irrespective of hierarchical order, and therefore, λ is the stretch along the fiber direction. $\mathbf{C} = \mathbf{F}^{\mathrm{T}}\mathbf{F}$ is the right Cauchy–Green deformation tensor, and $\mathbf{n}$ is the fiber direction in deformed configuration and is related to $\mathbf{n}_o$; the fiber direction in reference configuration is such that $\mathbf{n} = \frac{\mathbf{F}\mathbf{n}_o}{\lambda}$. At the fibril level, the multiplicative decomposition yields a generalized expression of the strain energy function (SEF) as

$$W_{\mathrm{fl}}\left(\bar{I}_{1e}, \bar{I}_{4e}\right) = \frac{1}{2}\mu^{\mathrm{fl}}\left(\bar{I}_{4e}\right)\left(\bar{I}_{1e} - 3\right) \tag{1}$$

where $I_{1e} = \lambda_{1e}^2 + 2\lambda_{1e}^{-1}$ and $\bar{I}_{4e} = \bar{\mathbf{C}}_e : \mathbf{n}_o \otimes \mathbf{n}_o$. The shear modulus, μ^{fl}, is a function of elastic fibril deformation and is expressed by

$$\mu^{\mathrm{fl}}\left(\bar{I}_{4e}\right) = \mu_o\left(\tanh\left[a_1\left(\bar{I}_{4e} - 1\right)\right] - a_2\exp\left[a_3\left(\bar{I}_{4e} - I_o\right)\right]\right) \tag{2}$$

Differentiating the strain energy with respect to $\bar{\mathbf{C}}_e$, the fibril stress under uniaxial tension can be expressed as

$$\sigma_{fl} = -p\mathbf{I} + \left(2\frac{\partial W_{fl}}{\partial \bar{I}_{1e}}\bar{\mathbf{B}}_e + 2\bar{I}_{4e}\frac{\partial W_{fl}}{\partial \bar{I}_{4e}}\mathbf{n}\otimes\mathbf{n}\right) \tag{3}$$

where $\bar{\mathbf{B}} = \bar{\mathbf{F}}_e\bar{\mathbf{F}}_e^{\mathrm{T}}$ is the left Cauchy–Green tensor, numerically equal to $\bar{\mathbf{C}}_e$.

The total strain energy for the fiber $\left(W_{\mathrm{fb}}\right)$ and tissue (W_t) formulation represented the combined axial and shear strains in both constituents. Satisfying the Clausius–Duhem dissipation inequality and the incompressibility constraint, the total stress σ^t was expressed with fibrillar σ^f and nonfibrillar σ^{nf} stress tensors as follows:

$$\begin{cases} \sigma^t = \sigma^{\mathrm{nf}} + \sum \sigma_i^f \\ \sigma^{\mathrm{nf}} = \frac{2}{J}\left(\bar{I}_1\frac{\partial W_t}{\partial \bar{I}_1}dev(\bar{\mathbf{B}}) + \left[E_k\bar{J}\left(\bar{J} - 1\right)\right]I\right) \\ \sigma_i^f = \left\{\frac{2}{J}\left(\bar{I}_4\frac{\partial W_t}{\partial \bar{I}_4}dev(\mathbf{n}\otimes\mathbf{n}) + \bar{I}_{4e}\frac{\partial W_t}{\partial \bar{I}_{4e}}dev\left(\mathbf{n_e}\otimes\mathbf{n_e}\right)\right)\right\}_i & \text{if } \bar{I}_{4i} > 1 \\ \sigma_i^f = 0 & \text{if } \bar{I}_{4i} \le 1 \end{cases} \tag{4}$$

The hierarchical mathematical expressions for the strain energy are shown in "Appendix A," and a more detailed description of the evolution of the constitutive model can be found in Adouni and Dhaher (2016), Tang et al. (2009).

2.3 Elastoplastic modeling of fibril

A collagen fibril, either native or degraded, exhibits elastoplastic behavior (Buehler 2006, 2008; Malaspina et al. 2017). One approach of representing the elastoplastic energetics is by employing a softening hyperelasticity (Volokh 2007a, b). Briefly, the softening of the fibril (plastic behavior) is captured by a constant Φ, *energy limiter*, defined as the critical failure energy or the maximum strain energy an infinitesimal volume of material can sustain without failure.

The limiter automatically induces stress bounds in the constitutive equations. Therefore, the fibril stress shown in Eq. (3) can be modified as follows:

$$\sigma_{\mathrm{fl}}^{\mathrm{SEF}} = -p\mathbf{I} + \left(2\frac{\partial W_{fl}}{\partial \bar{I}_{1e}}\mathbf{B_e} + 2\bar{I}_{4e}\frac{\partial W_{\mathrm{fl}}}{\partial \bar{I}_{4e}}\mathbf{n}\otimes\mathbf{n} \right) \exp\left(-\frac{W_{\mathrm{fl}}^{m}}{\Phi^{m}} \right) \tag{5}$$

where Φ and m are positive constants defined here in as tuning parameters and m is a dimensionless parameter that controls the sharpness of the transition from the elastic to the plastic behavior (softening).

The calibration process introduced in this work was strictly to map the MD simulation results to a continuum model of the fibril at different degradation levels using the formulation (Eq. 5) of fibril mechanics presented herein. The continuum-based formulation of the fibril mechanics was characterized by five parameters $(\mu_o, I_o, a_1, a_2, a_3)$. The total description of the constitutive model (Eq. 4) led to 13 unknown material parameters (Adouni and Dhaher), including these unknown five fibril parameters. In that study, the authors previously employed a Bayesian calibration approach to predict the evolution of the elastic fibril mechanical behavior (Adouni and Dhaher 2016; Salehghaffari and Dhaher 2015). The parameters were calibrated under the small axial strain (less than 10%) assumption, which could capture the elastic response of the native fibril. The plastic response of the native fibril expressed at large strains was characterized in terms of a single variable and was identified independent of the elastic response. However, the current study considered the degraded states of the fibrils, which resulted in simultaneous degradation-induced changes in the elastic and plastic responses (Malaspina et al. 2017). Hence, to capture the full range of strains and to capture the model parameters that will express both the elastic and plastic behaviors as a function of degradation, the softening hyperelasticity approached was employed and two more tuning variables were introduced as expressed in Eq. (5). A nonlinear optimization scheme was applied to compute the unknown fibril parameters from the modified fibril stress as shown in Eq. (5) for the mechanical response of both the native and degraded fibrils as computed by the MD simulation. For the nonlinear optimization, the input was the dataset obtained by MD simulation (stress–strain data) for each level of degradation for the two degradation mechanisms (surface and crosslink) considered in this study. The outputs of the optimization are the five fibril parameters: $\mu_o, I_o, a_1, a_2, a_3$. To ensure unbiased estimate of the fibril parameters $(\mu_o, I_o, a_1, a_2, a_3)$, multiple sets of the five fibril parameters selected from a plausible range of values were then used as the initial inputs to the optimization procedure. The multiple outcomes of the optimization process were then averaged to represent the best fit of the fibril parameters used to characterize the fibril continuum model employed in the subsequent FEA simulations. For each level of degradation (crosslink failure and surface degradation), a unique set of fibril parameters $(\mu_o, I_o, a_1, a_2, a_3)$ was estimated. Our choice of calibrating the "continuum-based" model of the fibril with data from MD simulation was due to the lack of experimental data on degraded fibril mechanics.

The incompressibility of the articular cartilage due to short-term (transient) biphasic response was imitated with an equivalent elastic response by using the equilibrium (drained) modulus of the tissue and Poisson's ratio of 0.5. The drained modulus was assumed to vary from 0.3 to 1.2 MPa with varying depth, when descending from the cartilage surface to the lowest layer at the subchondral bone, respectively (Schinagl et al. 1997). This led to the reduction in the numbers of unknown material parameters of the multiscale construct from 13 to 10. In addition to the fibril-level material responses (informed by MD simulation), we adopted the continuum-level material responses associated with the hierarchical composite model of the cartilage, which was calibrated using experimental data and was reported in a prior study from our group by Adouni and Dhaher (2016). The prior Adouni study leveraged experimental data reported by Akizuki et al. (1986), Eppell et al. (2006), Schinagl et al. (1997). It is important to note that the experimentally based calibrated parameters adopted here from the Adouni et al. study were consistent with the range of data used by other modeling-based research reports (Shirazi and Shirazi 2008; Guo et al. 2006; Tang et al. 2009).

2.4 Tissue-level synthesis: axisymmetric model

Validated finite element models of articular cartilage samples (plug) used in the reported experimental testing paradigms (Fig. 1a) were used here to facilitate cross-examining our results against experimentally similar indentation tests (Kerin et al. 1998; Spahn et al. 2007). In these simulations, the indenter was assumed to be a rigid body. The cylindrical plug of the articular cartilage was represented by an axisymmetric model, where the depth-dependent fibril networks at different regions were analogously considered. This axisymmetric parametric model resembles three-layered tissue morphology with depth-dependent orientation of fibers and its volume fractions, 15%, 18% and 21% in the superficial, transitional and deep zones, respectively, proposed in previous studies (Adouni et al. 2012; Shirazi et al. 2008; Wilson et al. 2004). We emulated enzyme-mediated degradation to collagen fibril in all layers to determine its aggregate effect on cartilage failure. The aggregate degradation due to the degenerated fibrils has been primarily evident at the superficial layer even though the degraded fibrils are distributed throughout the cartilage. The FE model of the cartilage tissue was constructed such that the hyperelastoplastic fibers

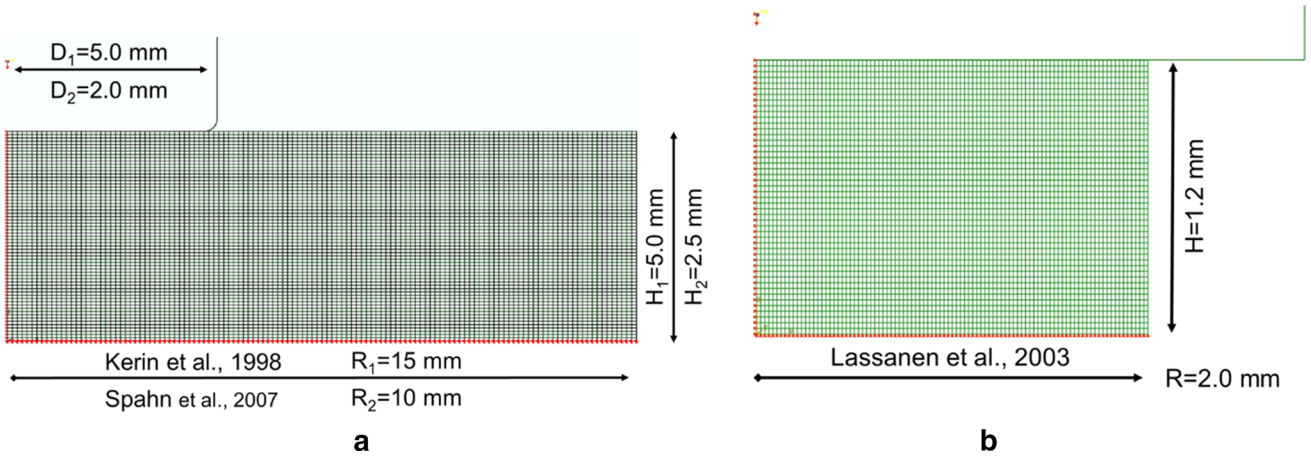

Fig. 1 Finite element models used to simulate the different experimental testing paradigms considered during this investigation; two indentation tests were used for the plastic damage (Kerin et al. 1998; Spahn et al. 2007) (**a**) and validation (Laasanen et al. 2003) (**b**)

were embedded in the hyperelastic matrix. Mesh size of the axisymmetric model was subjected to a sensitivity analysis until 5% difference in the reaction force was achieved.

3 Results

The kinematics of both native and degenerated collagen fibrils obtained by MD simulation was considered to determine the fibril material properties by nonlinear curve fitting of the MD simulation results. The stress–strain plots of MD simulation and its corresponding fitted curves for the two degeneration mechanisms are shown in "Appendix B." The mean values of the input parameters are summarized for both the degradation mechanisms in Table 1. The standard deviation resembles the spread of the parametric values.

The failure stress of the cartilage tissue with native fibril was ~31 MPa (Fig. 2a) when the specimen was exposed to an indentation force as reported by Kerin et al. (1998) (Fig. 1a), a value that was consistent with current simulation employing similar boundary conditions. Model predictions indicate that the failure stress progressively reduced with degradation, a near 50% reduction for a fibril void of any crosslinks and almost 52% for 3.3% of simulated surface degradation of the fibril. Spahn et al. (2007) experimental paradigm yielded a plastic damage initiation expressed near 30 MPa (Fig. 2b), consistent with model outcomes using identical specimen size and experimental boundary conditions. The model predictions indicated near 47% and 41% reduction in the tissue yield stress for a complete crosslink failure and maximum surface degradation for the conditions (Fig. 2b). The reduction in failure stress of the cartilage tissue indicates a generalized effect of fibril degeneration on the tissue.

Figure 3 shows the depth-dependent variation in aggregate cartilage damage for the degenerated fibrils. This figure represents the average von Mises stress across all elements for a given layer as a function of the bulk uniaxial applied compressive strain. While it is tempting to use the term "damage," the figure only shows the stress–strain curve (elastoplastic behavior) of a specimen when the embedded fibrils have experienced varying levels of degradation. The simulated indentation tests for both crosslink failure and surface degradation showed differential behavior when subjected to 40% axial strain. Figure 3a, b represents the von Mises stress at the superficial zone under the axial strain with degenerated fibril in terms of the percentage of intact crosslink (β_o) and surface degradation (δ). Figure 3c, d

Table 1 Fibril material parameters (Mean ± SD) obtained from the data fitting process

Materials parameters		Lower bound	Upper bound	Parametric values for crosslink failure	Parametric values for surface degradation
μ_o	Shear modulus of the fibril (MPa)	1000	4000	2718.913 (610.74)	2141.295 (818.131)
I_o	Secondary stiffening of the fibril	1.6	2.8	2.053 (0.314)	2.085 (0.385)
a_1	Dimensionless fibril parameter 1	0.1	2	0.938 (0.568)	1.16 (0.435)
a_2	Dimensionless fibril parameter 2	100	1000	379.367 (181.54)	464.592 (204.724)
a_3	Dimensionless fibril parameter 3	10	100	34.99 (10.084)	59.962 (20.238)

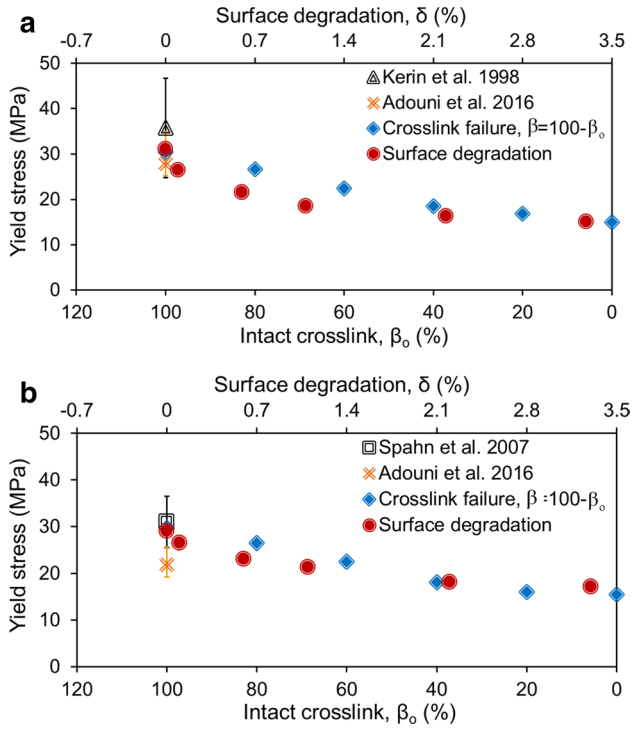

Fig. 2 Failure stress (experimental) of the articular cartilage (Kerin et al. 1998; Spahn et al. 2007) along with FE model prediction during simulated indentation test without degeneration (Adouni and Dhaher 2016) and with degeneration in terms of crosslink failure and surface degradation

mainly depicts the stress distribution at the middle zone for the two degeneration mechanisms. The gray vertical lines show the yield strains of fibrils varying between approximately 16% and 26% for crosslink failure and between ~ 24 and ~ 26% for surface degradation. All the stress–strain plots show toe regions, ~ 16 and ~ 19% for the superficial and middle layers, respectively, and a gradual transition into the linear region of stress–strain at the end of the toe region irrespective of the considered layers. The tissue-level yield strains varied between ~ 27 and ~ 37% for crosslink failure and ~ 30 and ~ 37% for surface degradation in the superficial layer, whereas no failure was observed at least up to 30% in the middle layer irrespective of the level of degradation and its type. Failure occurred nearly at the end of linear zone and resembled the tissue's ability to accommodate larger pre-yield strain. It was also evident that plastic deformation is less likely with depth. The cartilage tissue appeared to withstand more strain than the fibrils, and the middle and deep zones sustained even larger deformations before plastic changes took place.

Figure 4 shows the spatial distribution (propagation) of plastic changes (failure) of cartilage tissue in terms of fiber stretch, λ_{fp}, at yield during the simulated indentation test (Spahn et al. 2007) for both crosslink failure (Fig. 4a–f) and surface degradation (Fig. 4g–l). The stretch, λ_{fp}, is unity up to the yield point and only comes into play beyond the fiber yield strength. Plastic changes start at the superficial zone and propagate to the middle and deep zones, regardless of degradation mechanisms. The plastic change of the tissue with intact fibril is mostly confined within the superficial and partially in middle zones (Fig. 4a, b) but propagates to the deep zone partially as well with increasing fibril degeneration. The degradation was initiated from the central zone on the surface to the deep zone and spanned ~ 35% away from the axis of symmetry of the indenter for the native state and extended up to along the indenter edge with increasing degradation. However, the degradation extended ~ 10% more (Fig. 4f) beyond the indenter edge during crosslink failure. Our model simulations indicated that the spatial distribution of the plastic response of collagen fiber networks starts at superficial layer and then propagates to deep zone as well. However, the spatial distribution between the two types of degenerated fibrils resembles difference around the middle and (partially) in deep layers in comparison with the superficial layer. Figure 5 shows the von Mises stress map at the tissue level for both degradation mechanisms at different degradation levels and at the 40% applied bulk strain, with similar boundary condition used in the experiments carried by Spahn et al. (2007). In that experiment, the authors reported the failure stress in the surface layers of the specimens used. The maps shown in Fig. 5 indicate that, in some regions, the von Misses stress reaches the levels of "failure" stress reported in the aforementioned experiments, traditionally defined as a bulk level damage. It is important to note that while the local kinematics of fiber (stretch, Fig. 4) were significantly different when comparing the two types of degradation mechanisms, the tissue-level stress was nearly similar (Fig. 5). This also demonstrates that the mechanics of the matrix play a detrimental role and highlights the need for future work that incorporates ECM degradation models to evaluate the relative role of degradation of the two constituents on cartilage mechanics.

The aggregate behavior of the degraded cartilage model was compared to experimental data on modulus change post-collagenase—VII treatment (Laasanen et al. 2003). Laasanen et al. reported an average 70% change in cartilage equilibrium modulus after a treatment of collagenase applied to the surface layer of a cartilage sample. Translating the concentration of collagenase used by Laasanen et al. to the number of cleaved sites [expressed in terms of degradation percentages (δ)] at the fibril level used in the current model is not straightforward and required the introduction of basic assumptions. We employed a Langmuir surface adsorption model to the experimental data to compute fibril surface degradation associated with the collagenase treatment. We assumed an equal probability of enzyme adsorption to any fibril due to the high fibril density in the surface layer of

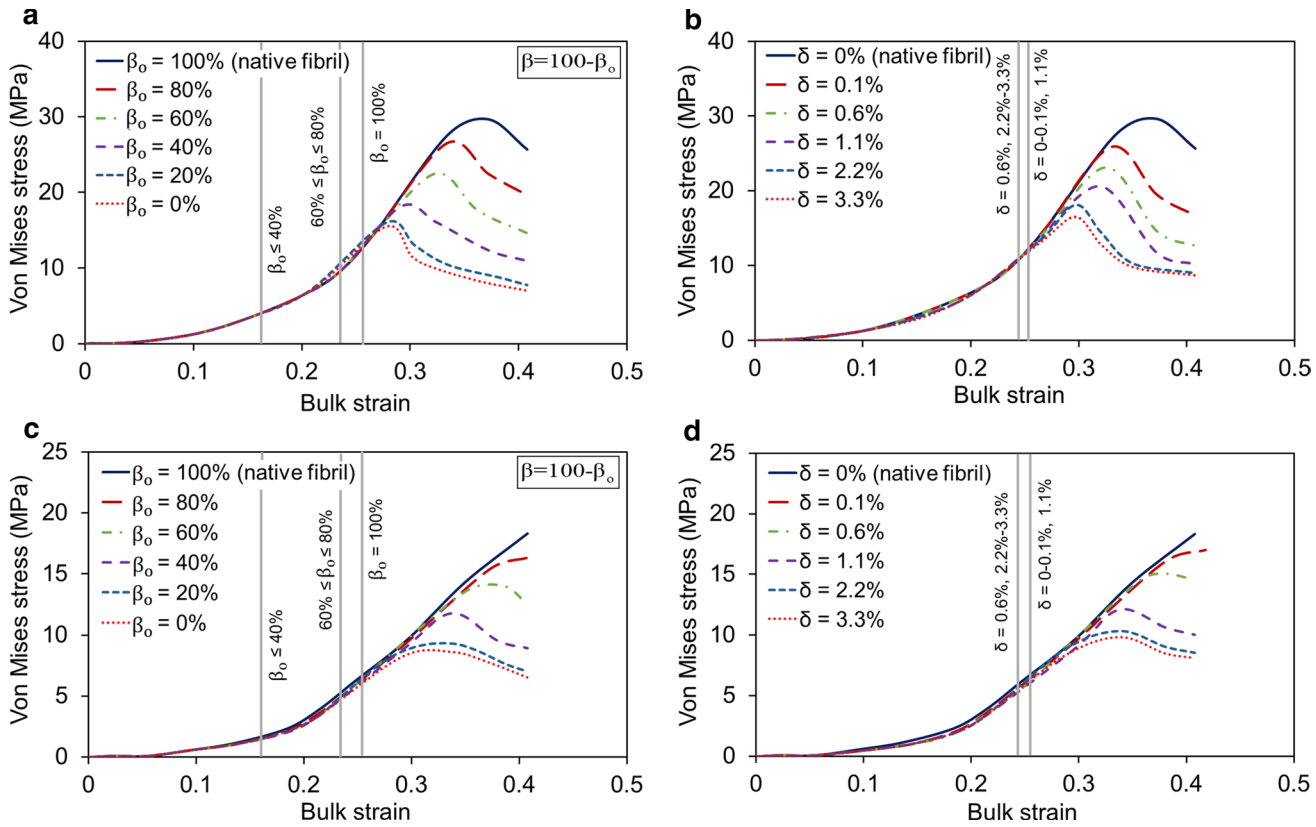

Fig. 3 Depth-dependent stress variation in articular cartilage as per the simulated indentation test (Spahn et al. 2007). Variation in von Mises stress at the superficial zone (**a**, **b**) and middle zone (**c**, **d**) with degeneration in terms of crosslink failure and surface degradation, respectively. Gray vertical lines denote fibril strain at yield (Malaspina et al. 2017)

the cartilage. A detailed description of the surface degradation estimation is presented in "Appendix C." Our estimate resulted in 1.75 ± 1.48 of surface degradation associated with the reported change in cartilage modulus (Laasanen et al. 2003) as shown in Fig. 6. Also shown in the figure is the computational model-based change in cartilage modulus (53.3 ± 11.4) for a theoretical surface degradation (δ) ranging from 0.02 to 3%. The range of the model predicted modulus falls within the spread of the estimated experimental change in equilibrium modulus.

4 Discussions

The objective of this study was to characterize the theoretical connection between tissue- and fibril-level mechanics in cartilage. We hypothesized that the integrity of fiber plays a significant role in the expression of tissue-level yield in the absence of a degraded matrix and the stabilizing effect of a nondegraded ECM at the tissue level depends on the degradation type experience by the fibrils. Our results indicate depth-dependent differences in the connection between fibril and tissue mechanical responses when a tissue specimen is subjected to an indentation load. While yield was expressed at the native fibril level at or near 25% strain (Malaspina et al. 2017), the yield strain was either larger (superficial layer) or absent (middle layer) at the tissue level. Our results indicate that plastic change was initiated at the superficial zone and subsequently propagated to the middle and deep zones. The ability of the cartilage to resist compressive load without failure reduced as the fibril degraded state increased independent of the degradation mechanism, surface (δ) or crosslink (β). Our degradation-based simulation results showed a change in the cartilage modulus consistent with the only experimentally reported change observed from a collagenase-treated cartilage samples (Laasanen et al. 2003). The study provided new insights into the role of fibrillar network and changes in its mechanics arising from the degenerative cascade at the fibril level that influences the aggregate tissue behavior. From a modeling prospective, the current model predicts the aggregate mechanics of the tissue due to an intrinsic to the tissue change, while most of the recent studies model cartilage response due to load-induced changes (Gardiner et al. 2016; Hosseini et al. 2014). Our interest has been to explore changes in the cartilage mechanics when fibrils undergo an enzymatically induced change

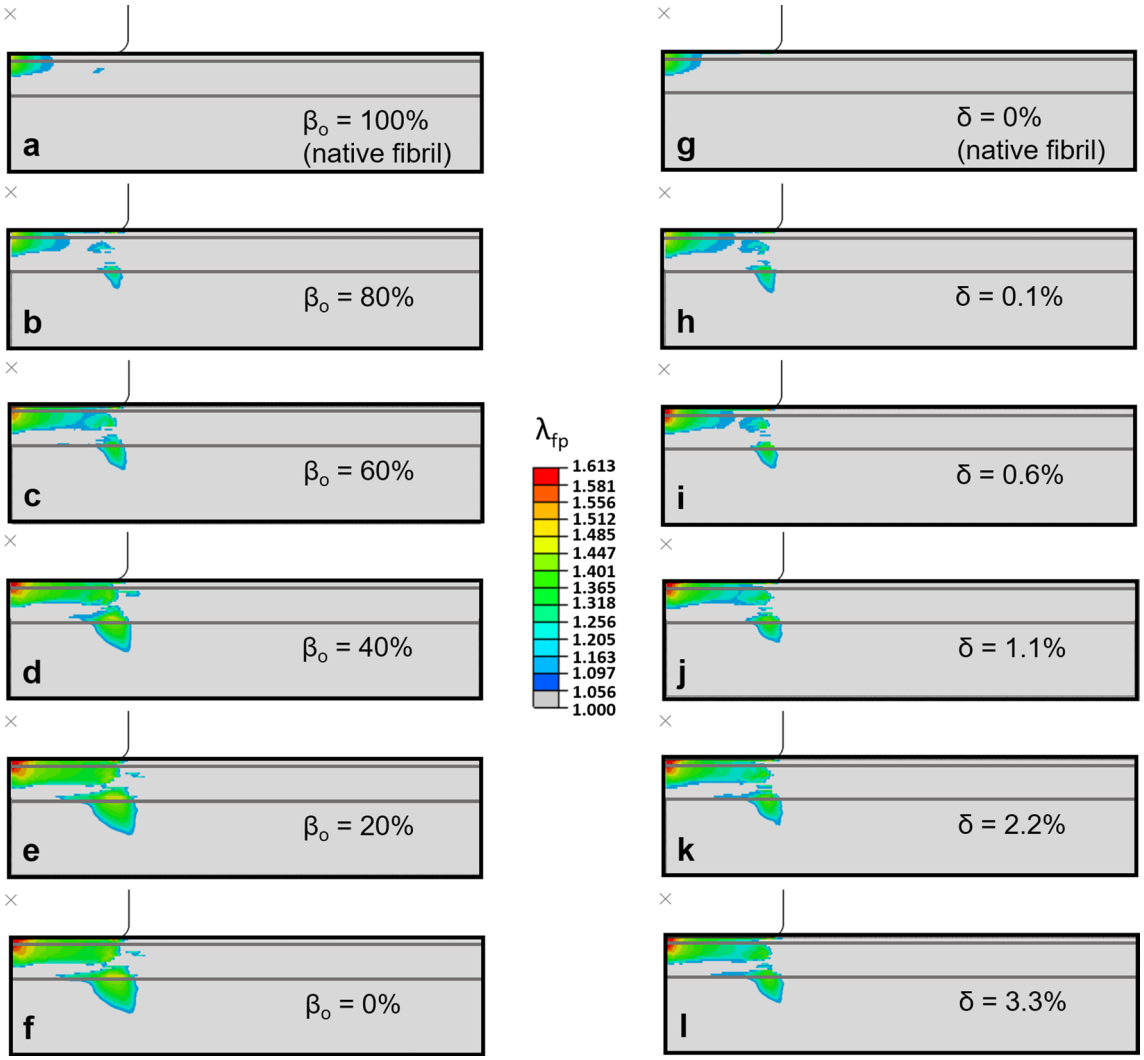

Fig. 4 Spatial distribution of cartilage tissue failure during the simulated indentation test (Spahn et al. 2007) with crosslink failure percentage of intact crosslink, β_o (**a**–**f**), where crosslink failure $\beta = 100 - \beta_o$ and surface degradation (**g**–**l**) subjected 40% of applied bulk strain. The spatial propagation was represented by the distributions of the maximum plastic fiber principal stretch (λ_{fp}), and a common legend is used for comparison. Gray horizontal lines show the divisions between the layers

in mechanics. The enzymatic effect employed here was emulated with an MD simulation process reported earlier from this group. In this work, we tried to explore if under an aggregate cartilage load, the degraded fibrils will experience a plastic state (post-yield). From an outcome prospective, our work signifies the key role ECM play in stabilizing the tissue even when the mechanics of the key constituent, collagen fibril, have been enzymatically compromised. While having a detrimental effect, the nature of the stabilizing role of the ECM varies depending on the nature of degradation (surface vs. crosslink). However, it remains to be seen if our findings are corroborated with experimental data explored simultaneously at the micro- and macroscales—data currently lacking in the literature. The differential response between collagen fibril and aggregate cartilage will help us to further explore the pathophysiological underpinnings of post-traumatic osteoarthritis and other forms of joint degeneration.

The spatial characteristics of the fibril network play a significant role in the expression of failure in the cartilage. While the yield strain at the native fiber level, as predicted by the MD simulation, was near ~ 25%, tissue-level simulation showed no yield behavior over the range of the applied strain in this layer. The randomness of the network in the middle layer makes the failure in this layer of the articular cartilage complicated and difficult to predict (Hong et al. 2015). Due to the randomized nature of the middle-layered fibers, the indentation load will likely not translate at the local level to axial loads long the fibrils. In the superficial layer, however, the tangential orientation of the fibrils exposes the fibrils to

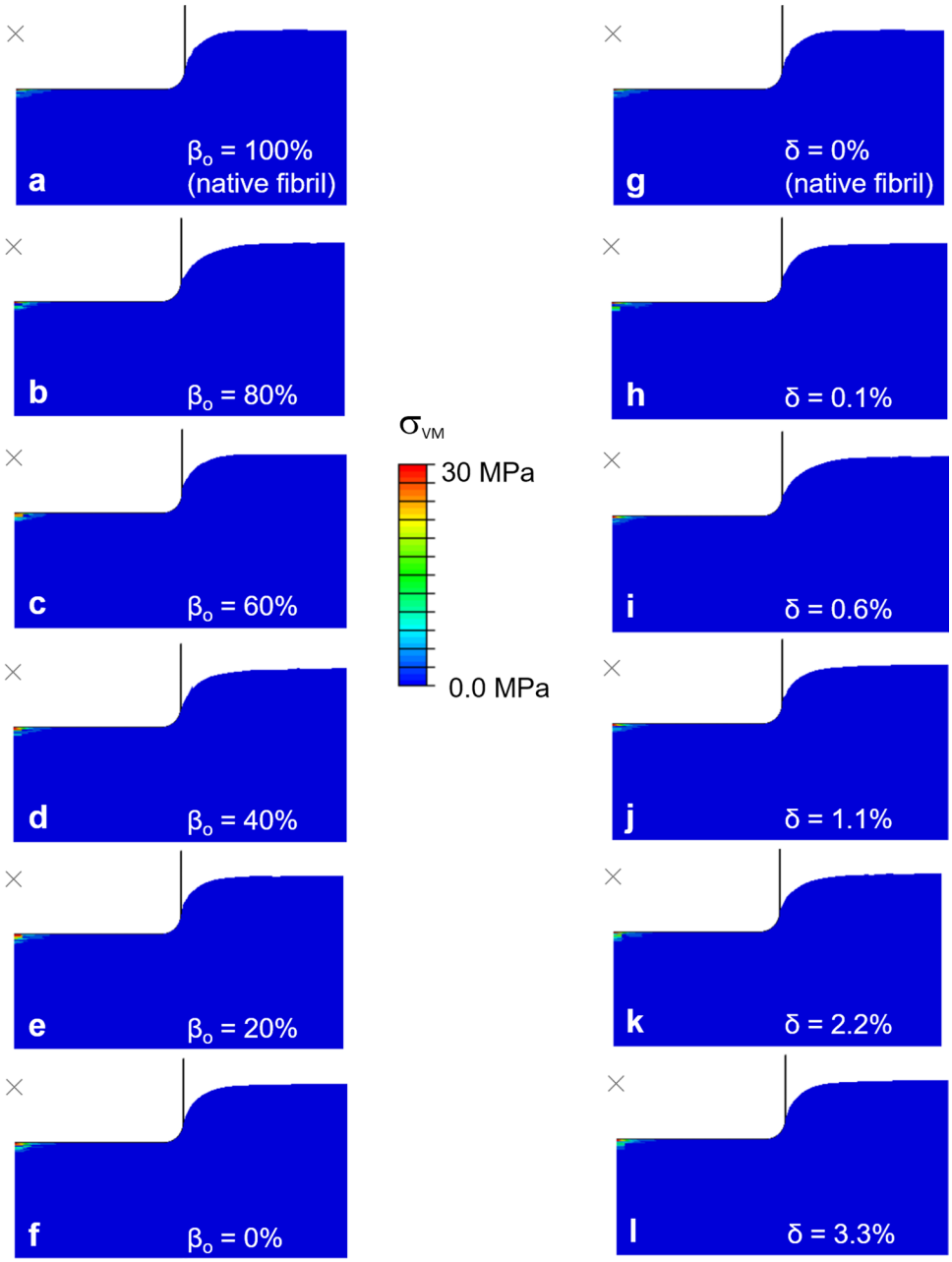

Fig. 5 Von Mises stress map (computed at the finite element level) for both crosslink failure (**a**–**f**) and surface degradation (**g**–**l**) mechanisms at different degradation levels and at the 40% applied bulk strain. The loading boundary condition is similar to the loading boundary condition used in the experiment by Spahn et al. (2007). While the geometric dimension is similar to Fig. 4, one-half of the model from the center of indentation has been shown for each case to clearly view the stress map

axial strains due to the transverse loading of indentation. Indeed, failure strain of the tissue at the superficial layer with the network of native tangentially oriented fibrils was 37%; in comparison, failure strain of the isolated native fibril under axial load was ~25%. However, the biomechanical function of cartilage is attributable to the tissue's extracellular matrix (ECM) (Maroudas 1976). Degradation of the ECM components and changes in their nanoscale structures significantly influence the macroscale behavior of the tissue and can ultimately result in loss of function with age and disease (Bonassar et al. 1995). While it is true that the mechanism of degradation at the fibril level (crosslink vs. surface) resulted in a uniquely different elastoplastic behavior (please see Fig. 8 in appendix), the general trends at the tissue level were similar. However, the notion of "a similar response" at the tissue level across the two different fibril degradation mechanisms may be misleading. The key difference between the two figures is related to the relative stabilizing role the ECM has on the tissue response when the collagen network is being degraded. For example, in the surface layer, the stabilizing effect of ECM resulted in a consistent shift in the expression of yield strain across degradation levels from what was computed at the fibril level for the crosslink case (~10%). Conversely, this effect changed as a function of the degradation level when the fibril underwent surface degradation (ranging from ~5 to ~12%). The observed stabilizing

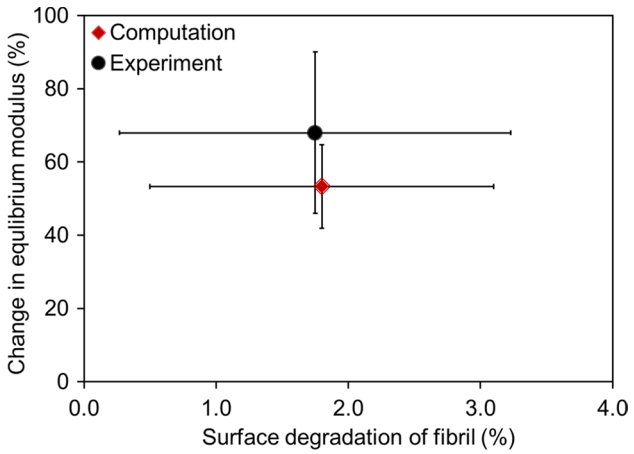

Fig. 6 Changes in equilibrium modulus of articular cartilage (mean ± SD) with respect to surface degradation due to the cleavage of collagen (by collagenase) during experiment (Laasanen et al. 2003) and computation. The vertical error bars represent the range of change of equilibrium modulus across specimens as reported by during the experiment. The horizontal bars indicate the estimated maximum and minimum bounds of degraded surface due to the collagen cleavage sites on the surface due to its exposure to collagenase

effect of ECM and its connection to the degradation type was consistent across layers. This observation demonstrates that the mechanics of the matrix play a detrimental role and highlights the need for future work that incorporates ECM degradation models (keeping with the theme of our approach, an enzymatically induced degradation model of the ECM) to evaluate the relative role of degradation of the two constituents on cartilage mechanics.

Our simulation results indicated a consistent shift in yield strain across degradation levels from what was computed at the fibril level for the crosslink failure. This may be due in part to the fact that removal of crosslinks (β) between the terminal ends of tropocollagen has limited effect on the elastic modulus of the fibril at the cartilage surface. In contrast, cleaving of tropocollagen molecules due to surface degradation (δ) of fibril results in a significant lowering of the yield strength of the fibrils (Panwar et al. 2013, 2015). One explanation may be that during surface degradation, the tropocollagen molecules are assumed to be mainly cleaved on the surface, which may result in irregular or asymmetric bonding between the surface molecules, with the load being carried out primarily by the intact core significantly compromising the fibril stiffness.

For both degradation types, yield strains were consistently higher in the middle layer compared to the superficial layer. Past studies support this finding, as prior experiments indicated that the middle layer of the cartilage requires the application of a larger bulk strain to express similar strain levels seen in the superficial layer when the tissue sample is exposed to lower levels of bulk strain (Chan et al. 2009, 2016; Neu and Walton 2008). However, while the effect on yield strain on the superficial layer was dependent on the degradation type, the type of degradation resulted in minimal differences in the yield behavior of the middle layer. Since load-bearing capacity of fibrils decreases with increasing degradation, the stiffness of fibrils reduces and concomitantly, superficial layer collapses under the indenter, transmitting plastic change (degradation) to the subsequent middle and deep zones. The spatial distribution of the plastic response seen herein is consistent with previous experiments that indicated fibrillation; clefts and disintegration of the collagen meshwork typically start at the superficial layer and then propagate to the deep layer (Clarke 1971; Saxena et al. 1991).

In this study, we employed a bottom-up approach to understand the effect of degradation of fibril network on cartilage failure. In the current context of this work, we assumed that all fibrils experience similar degradation state within and across layers, a limiting assumption of our model. Recall that any fibril degradation mediated by enzymatic processes depends on many factors including the diffusion of the enzymes into the cartilaginous tissue—a diffusion that may have spatial characteristics (Arbabi et al. 2015; Kar et al. 2016a; Li et al. 2015). However, our main goal was to express (aggregate) cartilage mechanics in response to mechanical changes at the fibril level as a result of enzymatic exposure. Driven by the need to understand OA diseases progression, limited computational attempts to model cartilage degradations have been reported in the literature (Adouni et al. 2012; Gardiner et al. 2016; Hosseini et al. 2014; Korhonen et al. 2015; Mononen et al. 2016). Unlike the current study, the degradation models proposed by the aforementioned studies focused primarily on load-induced degradation of the cartilage, reporting cartilage failure characteristics. Hosseini et al. (2014) presented a damage progression model of articular cartilage over time with repeated loading, defined by a set of degradation parameters. In the Hosseini and colleague model, a complete fiber failure was assumed at 18% strain, a value lower than the native fibril yield strain (~26%) derived from our earlier MD simulations and employed in the current model (Malaspina et al. 2017). Furthermore, Hosseini et al. (2014) reported that damage initiation was expressed at the deep layers prior to superficial layer expressed as a local strain of lower than 30%. In our examination, degradation started in the superficial layer at tissue strains ranging from 35% with native fibrils to ~25% for the degraded fibril, located underneath the indenter contact surface. Variations in predictions between the two models may be attributed in part to the different indenter shapes (flat vs. round), the inclusion of matrix failure model and the difference in the modeling paradigm. It can be construed that the primary contributor to the differences in the predicted failure patterns is due to the differences in the mechanism of

failure modeled, enzymatically mediated (current study) versus mechanically induced (Hosseini study). However, it may be argued that the inclusion of matrix degradation model will have a significant effect on the current model predictions of failure. Hosseini et al. suggest that both the intact fibrillar network and matrix may protect each other from developing damage, and that damage to either can promote cartilage failure. In the context of the bottom-up approach proposed herein, including MD-based characterization of failure of the proteoglycan network (matrix) is computational intractable. Key parameters of the energy potentials required for such simulations are unknown. It remains to be seen, however, if a future hybrid model of matrix (phenomenological) and fibril (MD) degradation will lead to different results.

Variation in failure stress in cartilage depends on many factors such as maturation, aging, location, collagen types and composition (Danso et al. 2014; Eleswarapu et al. 2011; Williamson et al. 2003). For example, tensile failure stress cartilage has been reported to range from 4.7 to 9 MPa (Danso et al. 2014; Williamson et al. 2003). Kerin et al. (1998) observed failure stress under compressive indentation ranging from 14 to 59 MPa, and Spahn et al. (2007) observed failure stress from 15.3 to 36.5 MPa. These variations are also seen across the different computational studies largely due to differences in the modeling approach used (Klets et al. 2016; Mononen et al. 2016; Peters et al. 2018). Mononen et al. (2016) computed fiber damage/softening when the tensile stress exceeds a threshold limit of 5–7 MPa. Hong et al. (2015) predicted collagen network damage near 45 MPa in the superficial layer. In the current work, the failure stress (under indentation) of the cartilage tissue varied from 31 MPa with native fibrils to 14.9 MPa for degraded fibrils. The variations in the predicted failure stress across these models may be attributed to model assumptions including fibrils buckling (Buckley et al. 2008; Nötzli and Clark 1997; Schinagl et al. 1997), fibril–fibril interactions (Broom and Silyn-Roberts 1989), fibril–matrix interactions (Maroudas 1976) and fluid pressurization (Ateshian 2009). In addition, fibril morphology and architecture, inclusion of secondary fibril, types of material modeling (i.e., hyperelasticity, viscoelasticity, poroelasticity) and collagen type-dependent mechanics may cause the differences in the mechanical properties and failure characteristics predicted by the current model with that of others.

The fibrillar mechanics used in this model was informed by MD simulations of collagen-I, typically found in ligaments (Buehler 2006, 2008; Malaspina et al. 2017). Collagen-II, on the other hand, is the main load-bearing collagenous component of cartilage (Mow et al. 1980). Although both types of collagen exhibit a similar, but not identical, nonlinear response to axial loading, experimental evidence demonstrates higher axial stiffness of heterotrimeric fibers (collagen-I) in comparison with homotrimeric fibers (collagen-II) (Kempson et al. 1968; Proctor et al. 1989). The difference in stiffness between these two types of fibers is attributed to the fibrillar architecture between the hetero- and homotrimeric TC molecules (Chang et al. 2012). Therefore, the model simulated in this study integrated the parameters trends that should be interpreted with care due to the differences in the collagen structure.

Conclusions derived herein depend on the validity of the model, and the presented model has not yet been validated thoroughly against experimental data. It is an extension of a prior model of a cartilage with intact fibril that was successfully cross-examined against data obtained using unconfined compression of cartilage specimens (see Fig. 2). Exploring the effect of degraded fibril on cartilage mechanics, on the other hand, is experimentally challenging. Our degradation-based simulation results, however, showed a change in the cartilage modulus consistent with the only experimentally reported change observed from a collagenase-treated cartilage samples (Laasanen et al. 2003). Translating the concentration of collagenase used by Laasanen et al. to the number of cleaved sites at the fibril level used in the current model for validation is, however, not straightforward and required the introduction of basic unverified assumptions. For example, we assumed that fibers are completely accessible to the enzyme (collagenases) and that the degradation percentages were uniformly distributed within and across the three layers of the cartilage. It has been reported that fibril degeneration is higher and localized to the tissue experienced excessive stress (Mononen et al. 2016). In addition, a number of reports indicate that collagen fibrils in cartilage are protected by the matrix (aggrecan) and the degradation of aggrecan with aggrecanase is a required precursor for the exposure of the fibrils to the collagenase (Kar et al. 2016b; Li et al. 2015; Pratta et al. 2003). In addition, both diffusion simulation and experiment verify that deep layer remains unaffected when a cartilage is treated with enzymes (Arbabi et al. 2015), and the fiber network may be mechanically compromised in the middle and deep level before any visible degradation becomes apparent at the surface (Hosseini et al. 2014). Future examinations incorporating a model for the matrix degradation and enzymatic diffusion into the cartilage will prove critical to our understanding of cartilage failure.

5 Conclusions

In this work, we explored the mechanical response of aggregate cartilage by introducing MD simulated degradation at the fibril level. Although the properties of cartilage tissue were largely contingent upon the mechanical properties of the depth-dependent fiber network, a distinctive deviation of the macroscale mechanics of the tissue was observed in the

simulated indentation tests. The aggregate behavior of tissue with native/intact fibril was nearly identical, but the fibril-level degradation mechanisms (crosslink failure and surface degradation) substantially and differentially influenced the kinematics of the aggregate cartilage. The magnitude and failure characteristics of the aggregate tissue noticeably differed from the micromechanical properties of fiber network. We found that fibril micromechanics are not the only predictor of aggregate tissue mechanics.

Acknowledgements The authors would like to thank Bethany Powell (PhD candidate) and David Malaspina (research fellow) in the Szleifer and Dhaher Labs at Northwestern University for the discussion in implementing surface adsorption to estimate surface degradation. The authors greatly appreciate the financial support of the National Institutes of Health for the Grant # U01 EB015410-01A1.

Compliance with ethical standards

Conflict of interest The authors declare no conflicts of interest.

Appendix A

Multiscale modeling of cartilage strain energy

In this study, the evolution of plastic stress in the fibril is triggered by the effective fibril yield stress derived from fibril strain energy (Tang et al. 2009). The yield stress is connected to the fibril yield condition as obtained from MDS (*i*), the plastic strain rate (*ii*) and the flow resistance (*iii*) of the tissues as follows:

$$\begin{cases} \sigma_y^{\text{eff}} = \frac{4}{3}\bar{I}_{4e}\frac{\partial W_{\text{fl}}}{\partial \bar{I}_{4e}} = \sigma^{\text{fl}}_{y(\beta)} \text{ and } \sigma^{\text{fl}}_{y(\delta)} & (i) \\ \dot{\gamma} = \dot{\gamma}_o \left|\frac{\sigma_{\text{eff}}}{\alpha(t)}\right|^{1/p} sig\left(\sigma_y^{\text{eff}}\right) & (ii) \\ \alpha(t) = \int h\dot{\gamma} f(\alpha) & (iii) \end{cases} \tag{6}$$

These relationships help describe the hierarchical coupling between nanoscale collagen degradation and material properties of fibrils (Fig. 6). The plastic parameters, $\dot{\gamma} = 0.01/\text{s}$ and $p = 0.05$, are fixed due to wide agreement in the literature with respect to cartilage's plastic rate of deformation (Gasser and Holzapfel 2002). A collagen fiber, which is modeled as the fiber-reinforced composite, includes the descriptions of fibril and incompressible neo-Hookean matrix. The elastic strain energy of the fiber can eventually be expressed under extension as

$$\begin{cases} W_{fbt}\left(\bar{I}_4, \bar{I}_{4e}\right) = v_{\text{fl}} W_{\text{fl}}\left(\bar{I}_{1ef}, \bar{I}_{4e}\right) + v_{ml}\left(\frac{\mu_{fm}}{2}\left(\bar{I}_{1f} - 3\right)\right) \\ W_{fs}\left(\bar{I}_{1f}, \bar{I}_4, \bar{I}_{4e}\right) = \frac{1}{2}\mu^{efffb}\left(\bar{I}_{4e}\right)\left(\bar{I}_{1fb} - \bar{I}_{1f}\right) \end{cases} \tag{7}$$

The total elastic strain energy density of the fiber is therefore expressed as

$$W_{fb}\left(\bar{I}_{1f}, \bar{I}_4, \bar{I}_{4e}\right) = W_{fbt}\left(\bar{I}_4, \bar{I}_{4e}\right) + W_{fs}\left(\bar{I}_{1f}, \bar{I}_4, \bar{I}_{4e}\right) \tag{8}$$

The framework is hierarchically used to model the soft tissue (cartilage) as the fiber-reinforced composite material as well, and the corresponding axial and shear strain energy are written as

$$\begin{cases} W_{tt}\left(\bar{I}_4, \bar{I}_{4e}\right) = v_f W_{fb}\left(\bar{I}_{1f}, \bar{I}_4, \bar{I}_{4e}\right) + v_m\left(\frac{\mu_m}{2}\left(\bar{I}_1 - 3\right)\right) \\ W_{ts}\left(\bar{I}_{1f}, \bar{I}_4, \bar{I}_{4e}\right) = \frac{1}{2}\mu^{\text{eff}}\left(\bar{I}_{4e}\right)\left(\bar{I}_1 - \bar{I}_{1f}\right) \end{cases} \tag{9}$$

The total strain energy of the tissue is defined by

$$W_t\left(\bar{I}_{1f}, \bar{I}_4, \bar{I}_{4e}\right) = W_{tt}\left(\bar{I}_4, \bar{I}_{4e}\right) + W_{ts}\left(\bar{I}_{1f}, \bar{I}_4, \bar{I}_{4e}\right) \tag{10}$$

The noticeable feature of the strain energy function is its dependence on both elastic stretch and the total deformation. This is due to the assumption that the plastic deformation occurs only in the fiber while the matrix materials always remain elastic. The total strain energy for the fiber (W_{fb}) and tissue (W_t) were therefore formulated mathematically combining axial and shear strains for the both, and eventually, the total stress σ^t was expressed with fibrillar σ^f and nonfibrillar σ^{nf} stress tensors as shown in Eq. (4) in the main article. The plastic stress in Eq. (4) becomes dominant when the effective stress, σ_y^{eff}, is more than the fibril yield strength, which in this case varies depending on the crosslink failure and surface degradation. The elastic part of the deformation gradient is determined by $\mathbf{F}_e = \mathbf{F}\mathbf{F}_p^{-1}$, where the plastic deformation gradient is $f\left(\lambda_{\text{fp}}\right)$. The stretch, λ_{fp}, is unity up to the yield point and only comes into play beyond the fiber yield strength. The plastic stretch depends on the plastic strain rate $\dot{\gamma}$, which ultimately controls the plastic part of the deformation gradient (Fig. 7).

Appendix B

Nonlinear optimization of degenerated fibril

The nonlinear optimization function *lsqnonlin* in MATLAB (The MathWorks Inc., Natick, MA, USA) was employed with the trust region reflective algorithm, which minimized an objective function $f(\mathbf{x})$ in a least square sense $\left(\sum_n \left[f(\mathbf{x})\right]^2\right)$. The optimal objective function provides a good compromise between $\sigma_{\text{fl}}^{\text{MDS}}$ (represents either $\left(\sigma_{fl}(\beta)\right)$ and $\left(\sigma_{fl}(\delta)\right)$ depending on degradation mechanisms, crosslink failure and generalized surface degradation, respectively) and $\sigma_{\text{fl}}^{\text{SEF}}$ for the fibril along the fiber direction,

$$f(\mathbf{x}) = \frac{\sigma_{\text{fl}}^{\text{SEF}}(\mathbf{x}) - \sigma_{\text{fl}}^{\text{MDS}}}{\sigma_{\text{fl}}^{\text{MDS}}} \tag{11}$$

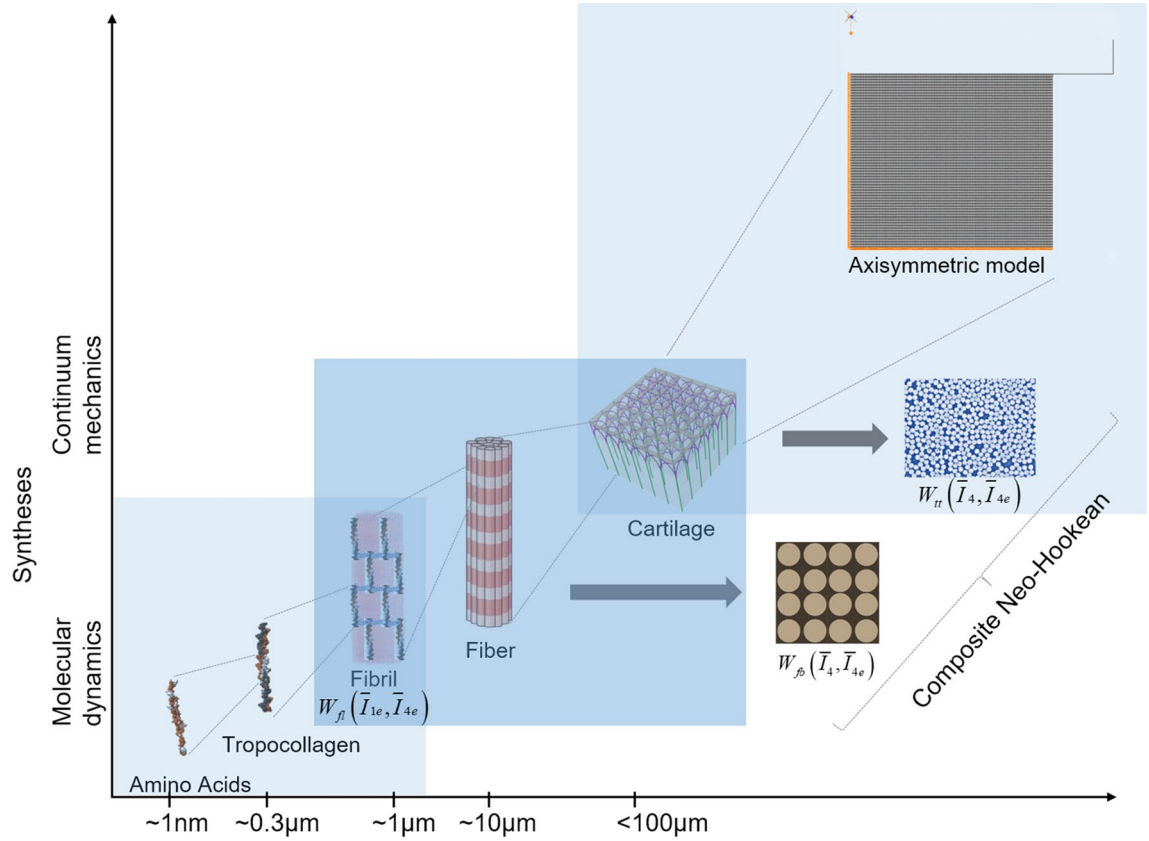

Fig. 7 Multiscale hierarchical organization of articular cartilage

where **x** is a vector of the unknown fibril parameters $\left(\mu_o, I_o, a_1, a_2, a_3\right)$ with each parameter confined by reasonable bounds as provided in earlier studies (Adouni and Dhaher 2016; Tang et al. 2009). To ensure unbiased estimate of the fibril parameters $\left(\mu_o, I_o, a_1, a_2, a_3\right)$, multiple sets of the five fibril parameters selected from a plausible range of values were then used (*MultiStart* MATLAB function) as the initial inputs to the optimization procedure. The multiple outcomes of the optimization process were then averaged to represent the best fit of the fibril parameters used to characterize the fibril continuum model employed in the subsequent FEA simulations.

Figure 8a displays the fibril stress–strain plot of MD data (solid line) and its corresponding fitted curve (dotted line) for the TC crosslink failure (β), varying from native fibril (100% crosslink) to no crosslink. Figure 8b shows the stress–strain curves (MD data and fitted curve) of a fibril at different levels of surface degradation (δ) varying from an intact fibril.

For the fitted data, the goodness-of-fit (GOF) values—coefficient of determination, R^2 (presented as mean ± standard error (SE))—were found 0.983 ± 0.04 for the crosslink failure and 0.978 ± 0.02 for the surface degradation. The fitted curves exhibit acceptable fits to the MDS data for the two degeneration mechanisms.

Appendix C

Estimation of surface degradation

The enzymatic surface degradation can be estimated based on the fraction of surface occupied by the adsorbate (enzyme). The accumulation of the adsorbate on a surface (adsorbent or substrate) is therefore known as adsorption. In the experiment carried out by Laasanen et al. (2003), collagenase type VII (C 0773, Sigma Chemical Co., St. Louis, MO, USA) was applied to degrade the surface of collagen-II in which surface degradation was estimated considering the binding of collagenase molecules on the collagen surface (Fig. 9). The incubation time (in 37 °C, 5% CO_2 atmosphere) for collagenase (30 U/ml)-treated samples was 44 h (Laasanen et al. 2003). Because of unavailability of specific parametric values, the surface coverage (degradation) was calculated using Langmuir adsorption isotherm for a range of physical

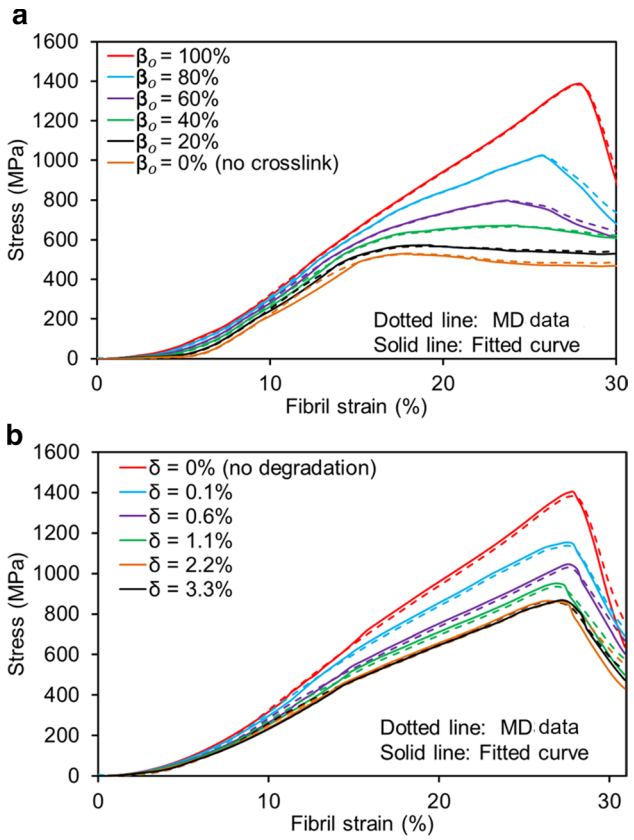

Fig. 8 Curve fitting by nonlinear optimization to MD simulation data to estimate input fibril parameters for **a** tropocollagen crosslink failure and **b** generalized surface degradation

and mechanical properties widely used for collagen and collagenase enzyme. The Langmuir adsorption isotherm provides one of the simplest and most direct methods to quantify the adsorption process. Since the Langmuir isotherm model typically well suited with isotherm data from protein/enzyme adsorption studies, the model is often used to estimate the protein binding affinity (Metzmacher et al. 2007a, b; Wilson et al. 2005).

Surface coverage

Surface coverage as per Langmuir Isotherm equation is

$$\theta = \frac{k_a C}{1 + k_a C} \tag{12}$$

where θ is the fractional surface coverage, C is the molar concentration of the solution (here collagenase VII), k_a is the association constant and k_d is the dissociation or binding constant. k_a and k_d are related as $k_a = \frac{1}{k_d}$.

The Collagen Digestion Unit (CDU) of the collagenase varies between 1000 and 3000 CDU/mg, and its molecular weight is between 68 and 125 kDa (Sigma-Aldrich; Webb 1992). For the ranges of CDU and molecular weight, the concentration, C, of collagenase (30 U/ml) was estimated in the range of $C = 0.08 \times 10^{-6} \sim 0.44 \times 10^{-6}$ mol/L.

The binding constant, k_d, between collagenase VII and collagen varies widely ($O(10^{-5})$ to $O(10^{-7})$) whether determined experimentally and computationally (Addi et al. 2016; Bella et al. 1994; Matsushita et al. 1998, 2001; Toyoshima et al. 2001). However, in most of the reported literature, k_d was estimated to be in the order of $O(10^{-6})$ (Bella et al. 1994; Evans 1981; Matsushita et al. 1998, 2001; Toyoshima et al. 2001; Wilson et al. 2003) and was used to calculate the surface coverage using Eq. (12). Considering $k_d = 4.99 \times 10^{-6}$ (Wilson et al. 2003), the fraction of binding sites on collagen occupied by collagenase was estimated to $\theta_{min} \cong 0.016$ and $\theta_{max} \cong 0.081$.

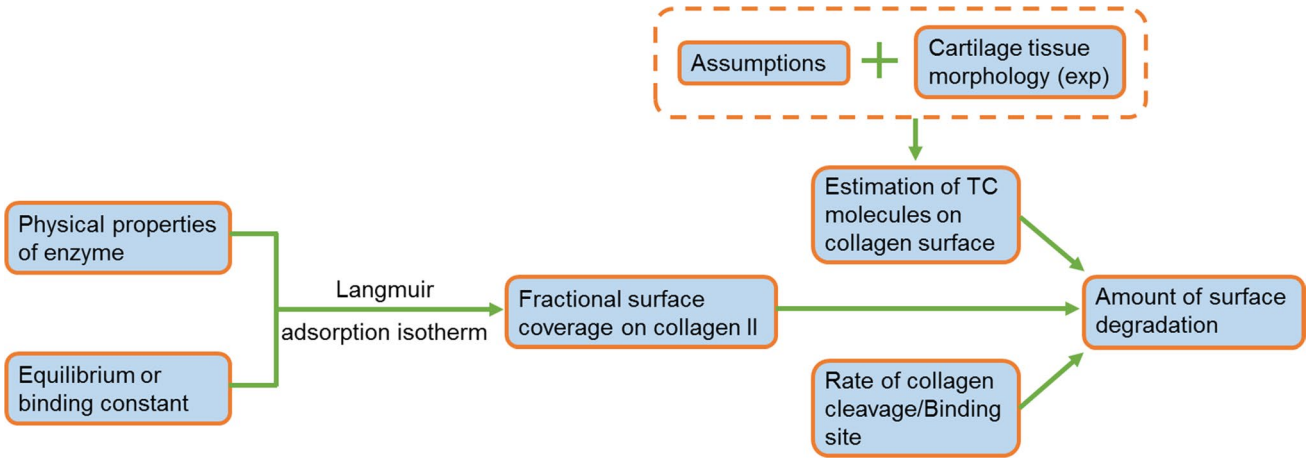

Fig. 9 Schematic of the estimation of surface degradation

Estimation of collagen fibrils in cartilage

The number of collagen fibril needs to estimate for the cartilage tissue used in the experiment (Laasanen et al. 2003). The following assumptions are rationally considered to calculate the amount of collagen fibrils in cartilage tissue:

1. Superficial layer or zone is typically 15% of articular cartilage tissue height $\left(h_{\text{tissue}}\right)$(Adouni et al. 2012; Hollander et al. 1994; Shirazi et al. 2008; Shirazi and Shirazi-Adl 2008).
2. Amount of collagen fibers in the superficial layer is approximately 15% (Adouni et al. 2012; Shirazi and Shirazi-Adl 2009; Shirazi et al. 2008).
3. Fibers are idealized as perfect cylinders of tightly packed monomeric fibrils
4. The fiber diameter is larger than the fibril diameter, $d_{\text{fb}} \gg d_{\text{fl}}$.
5. Diameter of a fiber $\left(d_{\text{fb}}\right)$ in cartilage generally in the range of $15.2 \pm 8.3 \sim 29.2 \pm 5.4$ nm (Halberg et al. 1988; Holmes and Kadler 2006; Moskowitz 2007; Mwenifumbo et al. 2007; Silver and Siperko 2003; Watanabe et al. 1994)
6. Length of the fiber is assumed to 1 μm (Domene et al. 2016; Gautieri et al. 2011; Liu et al. 2015)

An idealized fiber of tightly packed fibrils is shown in Fig. 10. This idealization is valid as long as the fiber diameter, d_{fb}, is much larger than the diameter of the fibril, d_{fl}. When the collagen fibrils come in contact with the enzyme solution, the enzyme diffuses into the fibers and binds to specific sites on fibrils located at the surface of the fibers. Due to the size and organization of the fibrils, the enzyme molecules cannot penetrate the tightly packed (crosslinked) fibrils that make up an individual fiber. The fibrils are also assumed to be incompressible and nonoverlapping (small circles in Fig. 10b).

Volume of sample cartilage plug, $V_{\text{tissue}} = \pi r^2 h\big|_{\text{tissue}} \approx 17.6\,\text{mm}^3$

Volume of the fibers in the superficial layer of the cartilage plug $\approx 0.4\,\text{mm}^3$

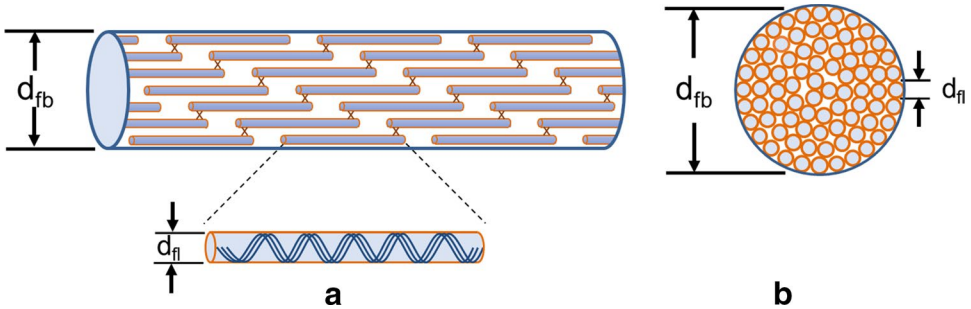

Fig. 10 Schematics of a fiber (**a**) and its cross section (**b**) perpendicular to the axis of the fiber [based on (Tzafriri et al. 2002)]

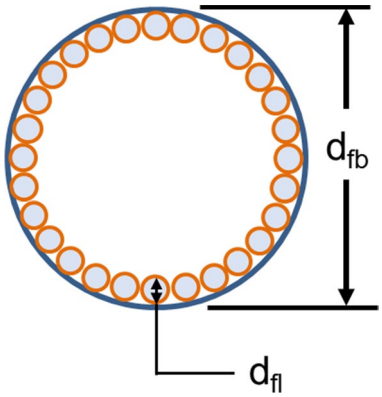

Fig. 11 Schematic of a fiber cross section perpendicular to the axis of the fibril showing TC molecules on the surface

Total number of collagen fibers is assumed to be n_{fb} that contribute to the total fiber volume. However, the fiber dimeter is variable depending on its young or mature state, and consequently, the diameters of fibers in the superficial layer vary widely (Moskowitz 2007; Mwenifumbo et al. 2007; Silver and Siperko 2003). Taking into account the minimum and maximum mean values of the fiber diameter, the minimum fiber volume, $V_{\text{fb}}^{\text{min}}$, and maximum fiber volume, $V_{\text{fb}}^{\text{max}}$, of a single collagen fiber have been estimated. Thus, based on the V_{fb}^{min} and $V_{\text{fb}}^{\text{max}}$, the minimum and maximum number of collagen fibers was estimated to $n_{\text{fb}}^{\text{min}} = 5.913 \times 10^{11}$ and $n_{\text{fb}}^{\text{max}} = 2.216 \times 10^{12}$, respectively.

Estimation of tropocollagen molecules on the surface

During the surface degradation process, enzymes bind and cleave the tropocollagen molecules on the surface (along the circumference of the fibril) and are schematically shown in Fig. 11. The TC molecules were assumed to be arranged tightly around the circumference of the fibrils. The dimensions of each TC molecule are $d_{\text{TC}} = 1.5\,\text{nm}$, $l_{\text{TC}} = 300\,\text{nm}$, with a ($D$-periodic) gap of 67 nm between the TC molecules (Chen et al. 1995; Franchi et al. 2007; Graham et al. 2004; Shoulders and Raines 2009).

Considering the minimum and maximum circumference of the fibers, staggered organization of TC molecules with the periodicity of 67 nm and (collagen type II) fiber length of 1 µm (Domene et al. 2016; Gautieri et al. 2011; Liu et al. 2015), the minimum and maximum number of TC molecules around the circumferential was estimated to $n^{\min}_{\mathrm{TC_{surf}}} = 5.68 \times 10^{13}$ and $n^{\max}_{\mathrm{TC_{surf}}} = 3.89 \times 10^{14}$.

Estimation of surface degradation

The collagenase type VII used in the Laasanen et al. experiments is bacterial collagenase, which acts both as a collagenase and a gelatinase. Collagenases can only cleave at one site on collagen molecules, but gelatinases can cleave the rest of the sites on the collagen once collagenase has made an initial cut. The bacterial collagenase can cut in multiple places on collagen and was accounted here for estimating the number of binding sites (Fig. 12). Thus, in the current estimation, we considered up to three binding sites/TC (Piluso et al. 2017; Riley and Herman 2005; Xu et al. 2000; Zderic 1995). Hence, the total number of collagenases on cartilage surface was estimated in the range of $n^{\mathrm{surface}}_{\mathrm{Collagenase}} \approx 2.726 \times 10^{12} \sim 9.453 \times 10^{13}$ molecules.

To the best of our knowledge (with extensive literature search), two different rates of collagen cleavage by the bacterial collagenase have been found and considered here in the estimation process. These are: (*i*) 22 molecules of collagen are degraded per molecule of collagenase per hour (Barrett et al. 2012; Welgus et al. 1980) and (*ii*) a unit of collagenase activity is defined to produce 10% cleavage of collagen in 2.5 h at 37° C (Zderic 1995).

Considering cleavage rate as per (*i*), the number of degraded molecules for 44 h of incubation time (Laasanen et al. 2003) was in the range of $n^{\mathrm{degraded\,mol}}_{\mathrm{collagen}} \approx 4.67 \times 10^{16} \sim 2.565 \times 10^{17}$ molecules. With this, the minimum and maximum surface degradation was estimated to 0.01% and 0.201%, respectively. According to cleavage rate as per (*ii*), the number of degraded molecules for the same incubation time (Laasanen et al. 2003) was in the range of $n^{\mathrm{degraded\,mol}}_{\mathrm{collagen}} \approx 3.0 \times 10^{15} \sim 2.054 \times 10^{16}$ molecules. With this, the minimum and maximum surface degradation was estimated to be 0.013% and 3.51%, respectively.

Although Langmuir adsorption isotherm is often considered to estimate the protein binding affinity, the Langmuir model does not take into account the interactions between enzymes—especially when the enzymes (considered as voluminous objects) are charged exhibiting enzyme-to-enzyme interactions and, in a context of a joint, exhibiting interactions with other molecules in the synovial fluid. Thus, the Langmuir model neglects any type of chemical interaction with the surroundings except the surface. Moreover, a fixed number of adsorption sites are typically approximated on a static surface under equilibrium conditions as per the Langmuir model. But, experimentally the surface of a collagen fibril is dynamic in nature since the number of adsorption sites changes with time as the degradation progresses, and thus, equilibrium is difficult to achieve. The Langmuir model, however, phenomenologically seems to capture the behavior of surface degradation and the associated adsorption sites that not only give a gross estimation of the amount of surface degradation but provide an insight into the degradation mechanisms as well.

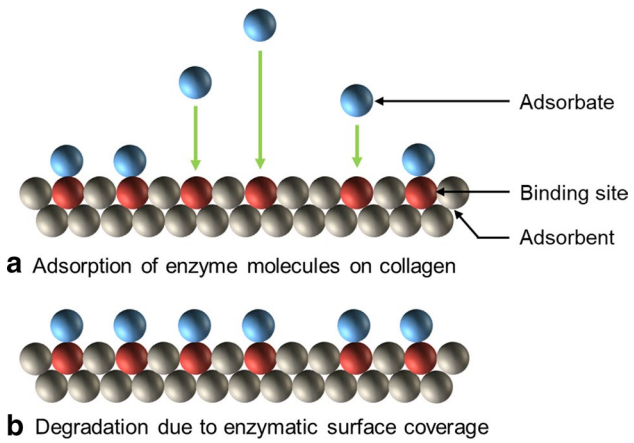

Fig. 12 Surface degradation due the cleavage of molecules by enzyme

References

Addi C, Murschel F, De Crescenzo G (2016) Design and use of chimeric proteins containing a collagen-binding domain for wound healing and bone regeneration. Tissue Eng Part B Rev 23:163–182

Adouni M, Dhaher YY (2016) A multi-scale elasto-plastic model of articular cartilage. J Biomech 49:2891–2898

Adouni M, Shirazi-Adl A, Shirazi R (2012) Computational biodynamics of human knee joint in gait: from muscle forces to cartilage stresses. J Biomech 45:2149–2156

Akizuki S, Mow VC, Müller F, Pita JC, Howell DS, Manicourt DH (1986) Tensile properties of human knee joint cartilage: I. Influence of ionic conditions, weight bearing, and fibrillation on the tensile modulus. J Orthop Res 4:379–392

Arbabi V, Pouran B, Weinans H, Zadpoor A (2015) Transport of neutral solute across articular cartilage: the role of zonal diffusivities. J Biomech Eng 137:071001

Asaro RJ, Rice JR (1977) Strain localization in ductile single crystals. J Mech Phys Solids 25:309–338

Ateshian GA (2009) The role of interstitial fluid pressurization in articular cartilage lubrication. J Biomech 42:1163–1176

Atkinson T, Haut R, Altiero N (1998) Impact-induced fissuring of articular cartilage: an investigation of failure criteria. J Biomech Eng 120:181–187

Backus JD et al (2011) Cartilage viability and catabolism in the intact porcine knee following transarticular impact loading with and without articular fracture. J Orthop Res 29:501–510

Bae WC, Lewis CW, Levenston ME, Sah RL (2006) Indentation testing of human articular cartilage: effects of probe tip geometry and indentation depth on intra-tissue strain. J Biomech 39:1039–1047

Bae WC, Schumacher BL, Sah RL (2007) Indentation probing of human articular cartilage: effect on chondrocyte viability. Osteoarthr Cartil 15:9–18

Barrett AJ, Rawlings ND, Woessner JF (2012) Handbook of proteolytic enzymes. Elsevier Science, New York

Bella J, Eaton M, Brodsky B, Berman H (1994) Crystal and molecular structure of a collagen-like peptide at 1.9 A resolution. Science 266:75–81

Bi X, Li G, Doty S, Camacho N (2005) A novel method for determination of collagen orientation in cartilage by Fourier transform infrared imaging spectroscopy (FT-IRIS). Osteoarthr Cartil 13:1050–1058

Bonassar LJ, Jeffries KA, Paguio CG, Grodzinsky AJ (1995) Cartilage degradation and associated changes in biomechanical and electromechanical properties. Acta Orthop Scand 66:38–44

Bozec L, Horton M (2005) Topography and mechanical properties of single molecules of type I collagen using atomic force microscopy. Biophys J 88:4223–4231

Broom ND, Silyn-Roberts H (1989) The three-dimensional 'knit' of collagen fibrils in articular cartilage. Connect Tissue Res 23:261–277

Brown TD, Johnston RC, Saltzman CL, Marsh JL, Buckwalter JA (2006) Posttraumatic osteoarthritis: a first estimate of incidence, prevalence, and burden of disease. J Orthop Trauma 20:739–744

Buckley MR, Gleghorn JP, Bonassar LJ, Cohen I (2008) Mapping the depth dependence of shear properties in articular cartilage. J Biomech 41:2430–2437

Buehler MJ (2006) Nature designs tough collagen: explaining the nanostructure of collagen fibrils. Proc Natl Acad Sci 103:12285–12290

Buehler MJ (2008) Nanomechanics of collagen fibrils under varying cross-link densities: atomistic and continuum studies. J Mech Behav Biomed Mater 1:59–67

Chan DD, Neu CP, Hull ML (2009) In situ deformation of cartilage in cyclically loaded tibiofemoral joints by displacement-encoded MRI. Osteoarthr Cartil 17:1461–1468

Chan DD, Cai L, Butz KD, Trippel SB, Nauman EA, Neu CP (2016) In vivo articular cartilage deformation: noninvasive quantification of intratissue strain during joint contact in the human knee. Sci Rep 6:19220. https://www.nature.com/articles/srep19220#supplementary-information

Chang S-W, Shefelbine Sandra J, Buehler Markus J (2012) Structural and mechanical differences between collagen homo- and heterotrimers: relevance for the molecular origin of brittle bone disease. Biophys J 102:640–648

Chen JM, Sheldon A, Pincus MR (1995) Three-dimensional energy-minimized model of human Type II "Smith" collagen microfibril. J Biomol Struct Dyn 12:1129–1159

Clarke IC (1971) Articular cartilage: a review and scanning electron microscope study. Bone Joint J 53:732–750

Danso EK, Honkanen JTJ, Saarakkala S, Korhonen RK (2014) Comparison of nonlinear mechanical properties of bovine articular cartilage and meniscus. J Biomech 47:200–206

Depalle B, Qin Z, Shefelbine SJ, Buehler MJ (2016) Large deformation mechanisms, plasticity, and failure of an individual collagen fibril with different mineral content. J Bone Miner Res 31:380–390

Domene C, Jorgensen C, Abbasi SW (2016) A perspective on structural and computational work on collagen. Phys Chem Chem Phys 18:24802–24811

Eleswarapu SV, Responte DJ, Athanasiou KA (2011) Tensile properties, collagen content, and crosslinks in connective tissues of the immature knee joint. PLoS ONE 6:e26178

Eppell SJ, Smith BN, Kahn H, Ballarini R (2006) Nano measurements with micro-devices: mechanical properties of hydrated collagen fibrils. J R Soc Interface 3:117–121

Evans CH (1981) Interactions of tervalent lanthanide ions with bacterial collagenase (clostridiopeptidase A). Biochem J 195:677–684

Franchi M, Trirè A, Quaranta M, Orsini E, Ottani V (2007) Collagen structure of tendon relates to function. Sci World J 7:404–420

Gardiner BS, Woodhouse FG, Besier TF, Grodzinsky AJ, Lloyd DG, Zhang L, Smith DW (2016) Predicting knee osteoarthritis. Ann Biomed Eng 44:222–233

Gasser TC, Holzapfel GA (2002) A rate-independent elastoplastic constitutive model for biological fiber-reinforced composites at finite strains: continuum basis, algorithmic formulation and finite element implementation. Comput Mech 29:340–360

Gautieri A, Vesentini S, Redaelli A, Buehler MJ (2011) Hierarchical structure and nanomechanics of collagen microfibrils from the atomistic scale up. Nano Lett 11:757–766

Graham JS, Vomund AN, Phillips CL, Grandbois M (2004) Structural changes in human type I collagen fibrils investigated by force spectroscopy. Exp Cell Res 299:335–342

Halberg D, Proulx G, Doege K, Yamada Y, Drickamer K (1988) A segment of the cartilage proteoglycan core protein has lectin-like activity. J Biol Chem 263:9486–9490

Haut R, Ide T, De Camp C (1995) Mechanical responses of the rabbit patello-femoral joint to blunt impact. J Biomech Eng 117:402–408

Hayes WC, Keer LM, Herrmann G, Mockros LF (1972) A mathematical analysis for indentation tests of articular cartilage. J Biomech 5:541–551

Hollander AP, Heathfield TF, Webber C, Iwata Y, Bourne R, Rorabeck C, Poole AR (1994) Increased damage to type II collagen in osteoarthritic articular cartilage detected by a new immunoassay. J Clin Investig 93:1722

Holmes DF, Kadler KE (2006) The 10 + 4 microfibril structure of thin cartilage fibrils. Proc Natl Acad Sci 103:17249–17254

Hong J, Evans TM, Mente PL (2015) Study on the damage mechanism of articular cartilage based on the fluid–solid coupled particle model. Adv Mech Eng 7:1687814015581264

Hosseini S, Wilson W, Ito K, Van Donkelaar C (2014) A numerical model to study mechanically induced initiation and progression of damage in articular cartilage. Osteoarthr Cartil 22:95–103

Huebner JL, Williams JM, Deberg M, Henrotin Y, Kraus VB (2010) Collagen fibril disruption occurs early in primary guinea pig knee osteoarthritis osteoarthritis and cartilage/OARS. Osteoarthr Res Soc 18:397–405

Julkunen P, Wilson W, Jurvelin JS, Rieppo J, Qu C-J, Lammi MJ, Korhonen RK (2008) Stress–relaxation of human patellar articular cartilage in unconfined compression: prediction of mechanical response by tissue composition and structure. J Biomech 41:1978–1986

Julkunen P, Wilson W, Isaksson H, Jurvelin JS, Herzog W, Korhonen RK (2013) A review of the combination of experimental measurements and fibril-reinforced modeling for investigation of articular cartilage and chondrocyte response to loading. Comput Math Methods Med 2013:1–23

Kar S, Smith DW, Gardiner BS, Grodzinsky AJ (2016a) Systems based study of the therapeutic potential of small charged molecules for the inhibition of IL-1 mediated cartilage degradation. PLOS ONE 11:e0168047

Kar S, Smith DW, Gardiner BS, Li Y, Wang Y, Grodzinsky AJ (2016b) Modeling IL-1 induced degradation of articular cartilage. Arch Biochem Biophys 594:37–53

Kaukinen A, Laasanen M, Lammentausta E, Halmesmäki E, Helminen H, Jurvelin J, Rieppo J (2005) Destructive testing of articular cartilage in compression-effect of collagen network. In: 51st Annual meeting of the orthopaedic research society

Kempson GE, Freeman MAR, Swanson SAV (1968) Tensile properties of articular cartilage. Nature 220:1127

Kerin AJ, Wisnom MR, Adams MA (1998) The compressive strength of articular cartilage. Proc Inst Mech Eng Part H J Eng Med 212:273–280

Klets O, Mononen ME, Tanska P, Nieminen MT, Korhonen RK, Saarakkala S (2016) Comparison of different material models of articular cartilage in 3D computational modeling of the knee: data from the Osteoarthritis Initiative (OAI). J Biomech 49:3891–3900

Korhonen RK, Tanska P, Kaartinen SM, Fick JM, Mononen ME (2015) New concept to restore normal cell responses in osteoarthritic knee joint cartilage. Exerc Sport Sci Rev 43:143–152

Laasanen M et al (2003) Biomechanical properties of knee articular cartilage. Biorheology 40:133–140

Lee EH (1969) Elastic-plastic deformation at finite strains. J Appl Mech 36:1–6

Li Y, Wang Y, Chubinskaya S, Schoeberl B, Florine E, Kopesky P, Grodzinsky AJ (2015) Effects of insulin-like growth factor-1 and dexamethasone on cytokine-challenged cartilage: relevance to post traumatic osteoarthritis osteoarthritis and cartilage/OARS. Osteoarthr Res Soc 23:266–274

Liu Y, Chan JK, Teoh SH (2015) Review of vascularised bone tissue-engineering strategies with a focus on co-culture systems. J Tissue Eng Regen Med 9:85–105

Lotz M (2001) Cytokines in cartilage injury and repair. Clin Orthop Relat Res 391:S108–S115

Malaspina DC, Szleifer I, Dhaher Y (2017) Mechanical properties of a collagen fibril under simulated degradation. J Mech Behav Biomed Mater 75:549–557

Maroudas A (1976) Balance between swelling pressure and collagen tension in normal and degenerate cartilage. Nature 260:808

Matsushita O, Jung C-M, Minami J, Katayama S, Nishi N, Okabe A (1998) A study of the collagen-binding domain of a 116-kDa Clostridium histolyticum collagenase. J Biol Chem 273:3643–3648

Matsushita O, Koide T, Kobayashi R, Nagata K, Okabe A (2001) Substrate recognition by the collagen-binding domain of Clostridium histolyticum class I collagenase. J Biol Chem 276:8761–8770

Metzmacher I, Radu F, Bause M, Knabner P, Friess W (2007a) A model describing the effect of enzymatic degradation on drug release from collagen minirods. Eur J Pharm Biopharm 67:349–360

Metzmacher I, Ruth P, Abel M, Friess W (2007b) In vitro binding of matrix metalloproteinase-2 (MMP-2), MMP-9, and bacterial collagenase on collagenous wound dressings. Wound Repair Regen 15:549–555

Miyazaki H, Hayashi K (1999) Tensile tests of collagen fibers obtained from the rabbit patellar tendon. Biomed Microdevice 2:151–157

Mononen ME, Tanska P, Isaksson H, Korhonen RK (2016) A novel method to simulate the progression of collagen degeneration of cartilage in the knee: data from the osteoarthritis initiative. Sci Rep 6:21415

Moskowitz RW (2007) Osteoarthritis: diagnosis and medical/surgical management. Lippincott Williams & Wilkins, Philadelphia

Mow VC, Kuei SC, Lai WM, Armstrong CG (1980) Biphasic creep and stress relaxation of articular cartilage in compression: theory and experiments. J Biomech Eng 102:73–84

Muthuri S, McWilliams D, Doherty M, Zhang W (2011) History of knee injuries and knee osteoarthritis: a meta-analysis of observational studies. Osteoarthr Cartil 19:1286–1293

Mwenifumbo S, Shaffer MS, Stevens MM (2007) Exploring cellular behaviour with multi-walled carbon nanotube constructs. J Mater Chem 17:1894–1902

Neu CP, Walton JH (2008) Displacement encoding for the measurement of cartilage deformation. Magn Reson Med 59:149–155

Newberry WN, Mackenzie CD, Haut RC (1998) Blunt impact causes changes in bone and cartilage in a regularly exercised animal model. J Orthop Res 16:348–354

Nötzli H, Clark J (1997) Deformation of loaded articular cartilage prepared for scanning electron microscopy with rapid freezing and freeze-substitution fixation. J Orthop Res 15:76–86

Oyen ML, Shean TA, Strange DG, Galli M (2012) Size effects in indentation of hydrated biological tissues. J Mater Res 27:245–255

Panwar P, Du X, Sharma V, Lamour G, Castro M, Li H, Brömme D (2013) Effects of cysteine proteases on the structural and mechanical properties of collagen fibers. J Biol Chem 288:5940–5950

Panwar P, Lamour G, Mackenzie NCW, Yang H, Ko F, Li H, Brömme D (2015) Changes in structural-mechanical properties and degradability of collagen during aging-associated modifications. J Biol Chem 290:23291–23306

Peters AE, Akhtar R, Comerford EJ, Bates KT (2018) Tissue material properties and computational modelling of the human tibiofemoral joint: a critical review. PeerJ 6:e4298

Piluso S, Lendlein A, Neffe AT (2017) Enzymatic action as switch of bulk to surface degradation of clicked gelatin-based networks. Polym Adv Technol 28:1318–1324

Pratta MA et al (2003) Aggrecan protects cartilage collagen from proteolytic cleavage. J Biol Chem 278:45539–45545

Proctor CS, Schmidt MB, Whipple RR, Kelly MA, Mow VC (1989) Material properties of the normal medial bovine meniscus. J Orthop Res 7:771–782

Repo R, Finlay J (1977) Survival of articular cartilage after controlled impact. J Bone Joint Surg Am 59:1068–1076

Riley KN, Herman IM (2005) Collagenase promotes the cellular responses to injury and wound healing in vivo. J Burns Wounds 4:1–24

Salehghaffari S, Dhaher YY (2015) A phenomenological contact model: understanding the graft–tunnel interaction in anterior cruciate ligament reconstructive surgery. J Biomech 48:1844–1851

Saxena RK, Sahay KB, Guha SK (1991) Morphological changes in the bovine articular cartilage subjected to moderate and high loadings. Cells Tissues Organ 142:152–157

Schinagl RM, Gurskis D, Chen AC, Sah RL (1997) Depth-dependent confined compression modulus of full-thickness bovine articular cartilage. J Orthop Res 15:499–506

Shirazi R, Shirazi-Adl A (2008) Deep vertical collagen fibrils play a significant role in mechanics of articular cartilage. J Orthop Res 26:608–615

Shirazi R, Shirazi-Adl A (2009) Computational biomechanics of articular cartilage of human knee joint: effect of osteochondral defects. J Biomech 42:2458–2465

Shirazi R, Shirazi-Adl A, Hurtig M (2008) Role of cartilage collagen fibrils networks in knee joint biomechanics under compression. J Biomech 41:3340–3348

Shoulders MD, Raines RT (2009) Collagen structure and stability. Annu Rev Biochem 78:929–958

Sigma-Aldrich. Collagenase from Clostridium histolyticum. High purity, purified by chromatography, Type VII, ≥4 FALGPA units/mg solid, lyophilized powder, 1,000-3,000 CDU/mg solid (CDU = collagen digestion units). https://www.sigmaaldrich.com/catalog/product/sigma/c0773?lang=en&region=US

Silver FH, Siperko LM (2003) Mechanosensing and mechanochemical transduction: how is mechanical energy sensed and converted into chemical energy in an extracellular matrix? Crit Rev Biomed Eng 31:255–331

Spahn G, Kahl E, Klinger Hans M, Mückley T, Günther M, Hofmann Gunther O (2007) Mechanical behavior of intact and low-grade degenerated cartilage/Mechanische Eigenschaften von intaktem und niedriggradig geschädigtem Knorpel 52. Biomed Tech 52:216–222

Stolz M, Raiteri R, Daniels A, VanLandingham MR, Baschong W, Aebi U (2004) Dynamic elastic modulus of porcine articular cartilage determined at two different levels of tissue organization by indentation-type atomic force microscopy. Biophys J 86:3269–3283

Stolz M et al (2009) Early detection of aging cartilage and osteoarthritis in mice and patient samples using atomic force microscopy. Nat Nanotechnol 4:186

Tang H, Buehler MJ, Moran B (2009) A constitutive model of soft tissue: from nanoscale collagen to tissue continuum. Ann Biomed Eng 37:1117–1130

Tang Y, Ballarini R, Buehler MJ, Eppell SJ (2010) Deformation micromechanisms of collagen fibrils under uniaxial tension. J R Soc Interface 7:839–850

Thompson JR, Oegema JT, Lewis J, Wallace L (1991) Osteoarthrotic changes after acute transarticular load. An animal model. J Bone Joint Surg Am 73:990–1001

Thompson RC, Vener MJ, Griffiths HJ, Lewis JL, Oegema TR, Wallace L (1993) Scanning electron-microscopic and magnetic resonance-imaging studies of injuries to the patellofemoral joint after acute transarticular loading. JBJS 75:704–713

Toyoshima T, Matsushita O, Minami J, Nishi N, Okabe A, Itano T (2001) Collagen-binding domain of a Clostridium histolyticum collagenase exhibits a broad substrate spectrum both in vitro and in vivo. Connect Tissue Res 42:281–290

Tzafriri AR, Bercovier M, Parnas H (2002) Reaction diffusion model of the enzymatic erosion of insoluble fibrillar matrices. Biophys J 83:776–793

Verzijl N et al (2002) Crosslinking by advanced glycation end products increases the stiffness of the collagen network in human articular cartilage: a possible mechanism through which age is a risk factor for osteoarthritis. Arthritis Rheumatol 46:114–123

Volokh KY (2007a) Hyperelasticity with softening for modeling materials failure. J Mech Phys Solids 55:2237–2264

Volokh KY (2007b) Softening hyperelasticity for modeling material failure: analysis of cavitation in hydrostatic tension. Int J Solids Struct 44:5043–5055

Watanabe H, Kimata K, Line S, Strong D, L-y Gao, Kozak CA, Yamada Y (1994) Mouse cartilage matrix deficiency (CMD) caused by a 7 bp deletion in the aggrecan gene. Nature Genet 7:154–157

Webb EC (1992) Enzyme nomenclature 1992. Recommendations of the nomenclature committee of the international union of biochemistry and molecular biology on the nomenclature and classification of enzymes, vol 6. Academic Press, Cambridge

Welgus H, Jeffrey J, Stricklin G, Roswit W, Eisen A (1980) Characteristics of the action of human skin fibroblast collagenase on fibrillar collagen. J Biol Chem 255:6806–6813

Williamson AK, Chen AC, Masuda K, Thonar EJMA, Sah RL (2003) Tensile mechanical properties of bovine articular cartilage: variations with growth and relationships to collagen network components. J Orthop Res 21:872–880

Wilson JJ, Matsushita O, Okabe A, Sakon J (2003) A bacterial collagen-binding domain with novel calcium-binding motif controls domain orientation. EMBO J 22:1743–1752

Wilson W, van Donkelaar CC, van Rietbergen B, Ito K, Huiskes R (2004) Stresses in the local collagen network of articular cartilage: a poroviscoelastic fibril-reinforced finite element study. J Biomech 37:357–366

Wilson CJ, Clegg RE, Leavesley DI, Pearcy MJ (2005) Mediation of biomaterial–cell interactions by adsorbed proteins: a review. Tissue Eng 11:1–18

Xu Y et al (2000) Multiple binding sites in collagen type I for the integrins α1β1 and α2β1. J Biol Chem 275:38981–38989

Zderic SA (1995) Muscle, matrix, and bladder function. In: Zderic SA (ed) Advances in experimental medicine and biology, vol 385. Plenum Press, New York. https://nla.gov.au/nla.cat-vn950200